Low energy He^+ ion effects in Cu films

Molecular dynamics simulation in support of thermal helium desorption experiments

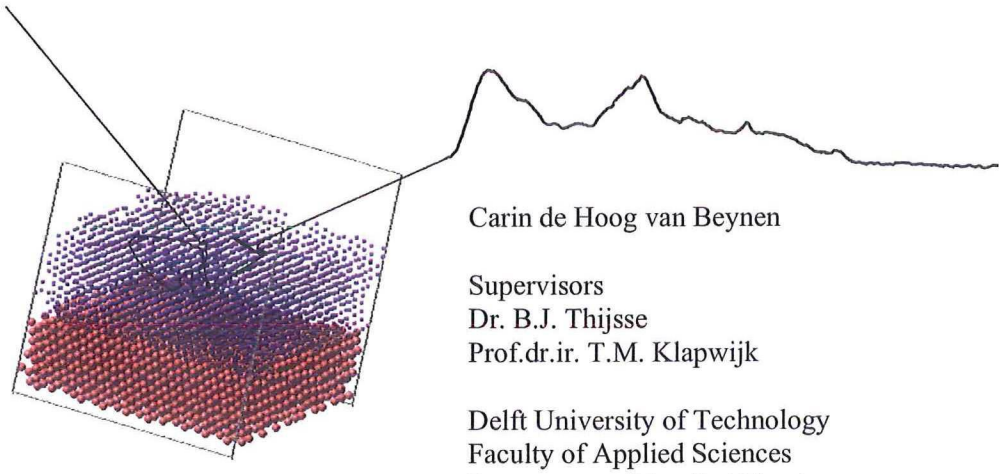

Carin de Hoog van Beynen

Supervisors
Dr. B.J. Thijsse
Prof.dr.ir. T.M. Klapwijk

Delft University of Technology
Faculty of Applied Sciences
Department of Applied Physics
Physical and Chemical Materials Science of
Dept. for Materials Science and Engineering
July 2000

Low energy He^+ ion effects in Cu films

Molecular dynamics simulation in support of thermal helium desorption experiments

Carin de Hoog van Beynen

Supervisors
Dr. B.J. Thijsse
Prof.dr.ir. T.M. Klapwijk

Delft University of Technology
Faculty of Applied Sciences
Department for Applied Physics
Physical and Chemical Materials Science of
Dept. for Materials Science and Engineering
July 2000

For my parents

Bij de interpretatie van meetresultaten speelt de weetonnauwkeurigheid soms een grotere rol dan de meetonnauwkeurigheid.
Stelling uit proefschrift van M.C.M.Bakker

Contents

1 Introduction

Defects in thin films

As miniaturization progresses, the properties of thin films are becoming increasingly important. Thin films are already found everywhere in today's life, for instance magnetic films for recording, and of course they are omnipresent in microelectronic devices. In physics and material science research on thin films is also 'hot'; researchers are very interested in nano- and microstructure of thin films and other phenomena on nanoscale. The microstructure of a film is of influence on most properties of thin films. In this study defects of various nature will be examined by means of atomistic computer simulations.

Defects in copper films

Copper is currently seen as a promising alternative for aluminum-based alloys in interconnects in integrated circuits [1]. The widths of interconnects become narrower resulting in the problem of electromigration. Copper is interesting for solving this problem due to its lower resistivity and superior resistance to electromigration. As defects such as vacancy clusters can frustrate both of these properties, it is important to know their behaviour, quantities, type and size. In this current work simulations are used to investigate defects in copper. Unfortunately Cu diffuses into silicon and silicon dioxide, and a good diffusion barrier is necessary. Tantalum (and alloys, nitrides and amorphous compounds of this material) is often mentioned [2, 3] as a candidate for diffusion barrier However, the Cu/Mo system will be studied here: molybdenum(110) as substrate for copper thin films. When the results of the Cu/Mo films are understood, the group (Physical and Chemical Materials Science) will continue with Cu/Ta and Cu/TaN films. Molybdenum is an appropriate first-stage model to Ta, because the materials are very similar but Mo lacks the complex crystal structure that forms in Ta under certain conditions. Also, the group has much experience with molybdenum both experimentally and in simulations. The Cu/Mo system is also interesting from a more fundamental point of view since Cu has a f.c.c. lattice and Mo a b.c.c. lattice. The influence of this interface on the microstructure and defects of the thin films is interesting to investigate.

The Cu/Mo films have been deposited with and without ion-beam assistance (Ion Beam Assisted Deposition). IBAD is a technique commonly used to influence the microstructure of thin films by bombarding the surface with ions during deposition, in our case low energy argon ions. With ion-beam assistance energy and momentum is added to the growing thin film, this can result in enhanced surface diffusion, sputtering and many other effects. Though this method produces several beneficial modifications in the properties of the grown films and is widely used, not all underlying mechanisms are fully understood. Also relatively little work has been published on the effect on defects in ion assisted grown films (see review on IBAD by Smith [4]). It is interesting to explore the ways in which defects and interface are different in films deposited with and without ion assistance.

Helium atoms as a probe for defects

Experimentally, a method capable of probing defects in films is thermal helium desorption spectrometry (THDS). A recording of the defect state of a film is obtained by bombarding the film with small, inert atoms at a low energy (in our case helium atoms). The He atoms can move interstitially through the lattice [5] and part of the helium atoms will be trapped in the defects of the thin film (defect 'decoration'). When the thin film is subsequently heated the He atoms detach from the defects by thermal vibrations and they escape through the surface (desorption). The number of escaping He atoms plotted against the temperature forms a THDS spectrum, from which the number and type of the defects in the thin film can be derived. The analysis of such a spectrum can be quite difficult.

In this research molecular dynamics simulations of this experimental method to probe defects are performed by bombarding Cu/Mo films with low energy He atoms. The objective is to gain more insight in the experimental spectra by simulating the defect probing by He atoms in the Cu/Mo films. The simulations can not only assist the interpretation of the THDS experiments, they also yield insight in show several interesting processes at atomic level such as the impacts of He atoms and motion of Cu atoms. In the simulations it is possible to look directly at atomic motion and structure i.e. local orientation, impact zones, local disorder, displacements of atoms, etc. Preliminary experimental results and simulations of the deposition with and without ion assistance of the Cu/Mo films already exist; they have been obtained as part of the ongoing research of our group. A key difference between the simulations of the experiments and the experiments is that only part of the experiments can be simulated. Simulation of desorption of the helium atoms from thin films is not feasible. The first part of the experiment, that is the decoration of the defects, can be simulated and provides information over defects in the film. This difference in simulation and experiment follows from the choice of method of simulation. Molecular dynamics simulations are limited in time scale and system size. This disadvantage does not apply to other methods such as Monte Carlo. This method however, needs an enormous amount of theoretical or experimental data about diffusion/interaction which were not available at the start of this research. Moreover, we are not only interested in the macroscopic characteristics of the system, but also in the dynamics of the impacting atoms in time. Other limitations of the molecular dynamics method of simulation originate from the choice of interaction potentials.

In Ch. 2 the limitations of the simulations and the experiments will be further discussed, preceded by a description of the simulation method and thermal desorption spectrometry. The Cu/Mo films are introduced in Ch. 3. In the second section of this chapter the scope of the simulations is given, i.e. the value ranges of variables such as the implantation energy, film thickness and growth method. Methods to reduce the limitations of time scale and system size are discussed in the last section of Ch. 3. The core of this research work follows in Ch. 4 and 5, in which the results of the simulated bombardments are presented, followed by a discussion of an interpretation of the experimental results with aid of these simulation results. In Ch. 6 conclusions and recommendations are given.

2 Methods

In this thesis TDS experiments are simulated with molecular dynamics to help interpret these experiments. The simulations will also give more direct information on the behaviour of the defects in the copper molybdenum thin films. In the first section the chosen method of simulation will be explained and specified. The second section will describe the not so common experimental technique Thermal Desorption Spectrometry. In both sections first the principles of the method will be explained followed by limitations of the method.

2.1 Simulation of TDS experiments

Principles

In molecular dynamics Newton's equations of motion are solved numerically for the individual particles of the system. The system consists of very large number of atoms or molecules; in our simulations the number of atoms varies from 4100 to 108000 atoms. From the individual positions, velocities and the interaction between the particles one can derive the macroscopic behaviour of the system such as temperature and pressure. However, we are not only interested in the macroscopic characteristics of the system, but also in the dynamics of the implanted atoms in time. Therefore molecular dynamics are used instead of Monte Carlo methods.

In order to find the time dependence of the position and velocity of the individual particles, we calculate the force $\vec{F}_i$ exerted on the ith atom, given by

$$\vec{F}_i = -\frac{dU(\vec{r}_1, \vec{r}_2, \ldots, \vec{r}_N)}{d\vec{r}_i} \tag{1}$$

in which $\vec{r}_i$ is the position vector of particle i and U is the total potential energy. This is genuinely a many-body expression for the force. With Newton's law '$F=ma$' the equations of motion for a particle i follow. Starting point of the simulation is the first configuration of the system (a list of position and velocity for each particle). For implementation in a computer programme it is necessary to discretize the time scale. The velocity Verlet algorithm [6] is used for this approximation, therefore the equations of motion of a particle i are given by

$$\vec{r}_i(t+\Delta t) = \vec{r}_i(t) + \vec{v}_i(t)\Delta t + \frac{1}{2m}(\Delta t)^2 \vec{F}_i(t), \tag{2}$$

$$\vec{v}_i\left(t+\tfrac{1}{2}\Delta t\right) = \vec{v}_i(t) + \frac{1}{2m}\Delta t \vec{F}_i(t), \tag{3}$$

$$\vec{v}_i(t+\Delta t) = \vec{v}_i\left(t+\tfrac{1}{2}\Delta t\right) + \frac{1}{2m}\Delta t \vec{F}_i(t+\Delta t), \tag{4}$$

in which Δt is the timestep, $\vec{v}_i(t)$ is the velocity of particle i at time t and $1/m \cdot \vec{F}_i(t)$ is the acceleration of particle i calculated from the positions at time t. With these equations of motion the positions, velocities and forces (new configuration) at time $t+\Delta t$ can be determined.

In our simulation we implant helium atoms at certain times and for a time these helium atoms have a huge velocity compared to the velocities of the copper and molybdenum atoms in the lattice. The initial high velocity of these helium atoms causes the timestep to become very small. This makes it inefficient to choose a fixed Δt for the entire simulation, so instead the timestep is chosen for each configuration. The timestep is chosen such that no atom moves more than a small, preset distance Δr (0.02 Å) over which the forces on the atoms do not change significantly. Atoms in free flight are excluded in the calculation of the timestep. The actual algorithm of this timestep is based on Eq. (2) and explained in Klaver [7].

From the preceding equations it is obvious that the choice of interaction potential is extremely important in molecular dynamics. For our simulations three interaction potentials to grow copper on a molybdenum substrate are needed: Cu-Cu, Mo-Mo, Cu-Mo and of course three interaction potentials to implant helium atoms: He-Cu, He-Mo and He-He. The potentials of argon with every other already mentioned element are also defined to simulate IBAD. The simulated system is quite complex and consists of many particles. Ab initio electronic-structure calculations for such a system are still too expensive in terms of computing time. Therefore, semi-empirical potentials are chosen to describe the interaction between the particles. A more detailed treatment of the successive potentials follows next. The Cu-Cu and Cu-Mo interaction potential functions were recently defined and Mo-Mo is not, for this reason the Mo-Mo interaction potential is less elaborately treated.

Cu-Cu interaction

Defects, the interface and the surface of the Cu/Mo system are the main interest of this thesis. The embedded-atom method (EAM) describes an interaction potential that also performs well in modeling inhomogeneities in the system such as the surface and defect structures [8]. In this method the energy of each atom is partly computed from the energy needed to embed the atom in the local electron density provided by the other atoms in the metal (first part of the equation) and partly from short-ranged electrostatic contributions due to electron cloud overlap (pair potential ϕ_{ij}). The EAM total potential energy is written as

$$U = \sum_i F_i(\rho_i) + \tfrac{1}{2}\sum_i \sum_{j \neq i} \phi_{ij}(r_{ij}), \tag{5}$$

where F_i is the embedding function. The electron density ρ_i that an atom i experiences is approximated by

$$\rho_i = \sum_{j \neq i} f_j(r_{ij}) \tag{6}$$

where f_j is the electron density at the position of atom i caused atom j. The angular dependence is averaged out, so that f_j is only dependent on the distance r_{ij} between the atoms i and j. Thus in the EAM method one uses electron densities without actually having electrons in the system. One of the consequences of not having electrons in the model is that heat diffuses more slowly than in reality, because there is no contribution from the electrons to the thermal conductivity. However, we use a special kind of temperature control: in each timestep the velocities of the atoms are scaled towards a desired temperature. This accounts for the fast thermal diffusivity of the conduction electrons.

Oh and Johnson [9] have chosen the functions

$$f(r) = f_e e^{-\beta\left(\frac{r}{r_{1e}}-1\right)}, \tag{7}$$

$$F(\rho) = a\left(\frac{\rho}{\rho_e}\right)^n + b\left(\frac{\rho}{\rho_e}\right), \tag{8}$$

$$\phi(r) = \phi_e e^{-\gamma\left(\frac{r}{r_{1e}}-1\right)} \tag{9}$$

for the electron density, the embedding function and the pair potential for close-packed metals. Here r_{1e} is the equilibrium first neighbour distance in the perfect crystal and from eq. (6) follows

$$\rho_e = \sum_m f(r_{me}) \tag{10}$$

where r_{me} is the distance to the mth neighbour of a particular atom in the equilibrium crystal. The functions $f(r)$ and $\phi(r)$ are smoothly cut off at a certain distance as in Oh and Johnson [9] to limit the number of interactions that are included in the calculations of the potential energy to reduce computing time. At cutoff distance r_c, $f(r_c) = f'(r_c) = 0$ and $\phi(r_c) = \phi'(r_c) = 0$, so that the interaction potential function is zero at r_c (here 4.86 Å).

The parameters f_e, β, a, b, n, ϕ_e and γ need yet to be determined. Except for f_e,, β and γ the parameters are fitted from five equations that couple EAM expressions to (experimental) values of copper. These equations relate the equilibrium properties of copper such as cohesive energy and bulk modulus to EAM expressions by applying an infinitesimal strain to perfect pure crystal at equilibrium. In these equations there is also an expression that relates information on a state that deviates slightly from the perfect copper crystal at equilibrium to EAM expressions through the unrelaxed vacancy formation energy equations (see exact functions and derivation Oh and Johnson [10 and 9]). The parameter f_e acts as an electron density scaling factor used when a interaction potential is defined for two different materials. For a monatomic material f_e can be given any value, because in the embedding function only ratios of ρ's occur. The values of parameters β and γ are chosen as by Oh and Johnson [9]. The experimental values for copper and the found EAM parameters used in the Cu-Cu potential are listed in Table I.

Apart from limiting the number of interactions that are included in the calculations of the interatomic potential function two other adjustments have been made: 1st the embedding function has been slightly altered near $\rho = 0$ as in Klaver [7] and 2nd the EAM potential has been replaced by a pair potential for very short range (high energy) interactions. The embedded atom method is used to simulate crystals. However, in this thesis we implant atoms at relatively high energies so it is also necessary to define the short-range interactions properly and this is done best with pair potentials. A screened Coulomb potential with Firsov screening length and Molière terms in the screening function [11] is used. This can be written in the form

$$\phi(r) = \frac{Z_1 Z_2 e^2}{4\pi\varepsilon_0 r} S\left(\frac{r}{a_F}\right), \tag{11}$$

where the Molière screening function $S(r/a_F)$ is given by

Table I. Used experimental values and EAM parameters of the EAM potentials for different interactions. Here a is the lattice parameter, E_c is the cohesive energy, $\langle B \rangle_V$ and $\langle G \rangle_V$ are the average Voigt bulk and shear moduli, E_v^{uf} is the unrelaxed vacancy formation energy, Ω is the atomic volume at equilibrium and A is the anisotropy ratio.

parameters	***Cu-Cu potential***	***Mo-Mo potential***
a (Å)	3.61496	3.1472 [7]
E_c (eV)	3.54 [10]	6.81 [13]
$\Omega \langle B \rangle_V$ (eV)	10.104 [12]	25.68 [13]
$\Omega \langle G \rangle_V$ (eV)	4.0278 [12]	12.28 [13]
E_v^{uf} (eV)	1.31 [10]	3.1 [13]
A	-	0.78 [7]
β	5 [9]	6 [13]
f_e	1 (used in Cu-Cu potential	1 (used in Mo-Mo potential)
	0.43 (used in Cu-Mo potential)	1 (used in Cu-Mo potential)
a (eV)	- 4.09728	-
b (eV)	- 1.70112	-
n	0.441494	-
γ	8.5 [9]	-
ϕ_e (eV)	0.369651	-
m (n in [7,13])	-	0.592708
K_0 (eV)	-	-0.45159
K_1 (eV)	-	-1.65312
K_2 (eV)	-	11.58783
K_3 (eV)	-	-0.32467

$$S\left(\frac{r}{a_F}\right) = 0.35e^{-0.3\frac{r}{a_F}} + 0.55e^{-1.2\frac{r}{a_F}} + 0.1e^{-6.0\frac{r}{a_F}}, \tag{12}$$

and the Firsov screening length is given by

$$a_F = \left(\frac{9\pi^2}{128}\right)^{\frac{1}{3}} a_B \left(Z_1^{\frac{1}{2}} + Z_2^{\frac{1}{2}}\right)^{-\frac{2}{3}} \tag{13}$$

where a_B is Bohr radius, Z_1 and Z_2 are the atom numbers of the interacting particles. This potential function is used for $r \leq 1.34$ Å. At this point there has to be a smooth transition between the pair potential and the EAM energy. Therefore, the same mechanism is used as in Klaver [7] where the Firsov Molière potential is smoothly connected to the pair potential of the EAM potential. Near r = 1.34 Å the electron density (and hence the embedding contribution) has been forced to fall off to zero due to multiplication with a Fermi-Dirac-like smooth step function. The interatomic potential function for two copper atoms is depicted in fig. 1.

The activation energy for the vacancy diffusion of bulk copper in the simulations is 0.77 ± 0.10 eV and the vacancy formation energy is 1.3 eV, both are in agreement with the usual literature data. The adatom migration energy on a (111) Cu surface is 0.057 eV in the simulations in the temperature range of 300-1200 K calculated by counting the number of

atomic jumps. If the mean square displacement is used for the determination of the same value, the adatom migration energy is 0.082 eV. There is reasonable resemblance with values mentioned by Wang, Li and Adams [14 and 15], respectively 0.026 eV and ~0.085 eV (value is derived from Fig. 8 from the article). See for more data [16]. This Cu-Cu interaction potential results in a 6% too low density of ideal bulk copper at 300 K. The Cu-Cu interaction seems to work well.

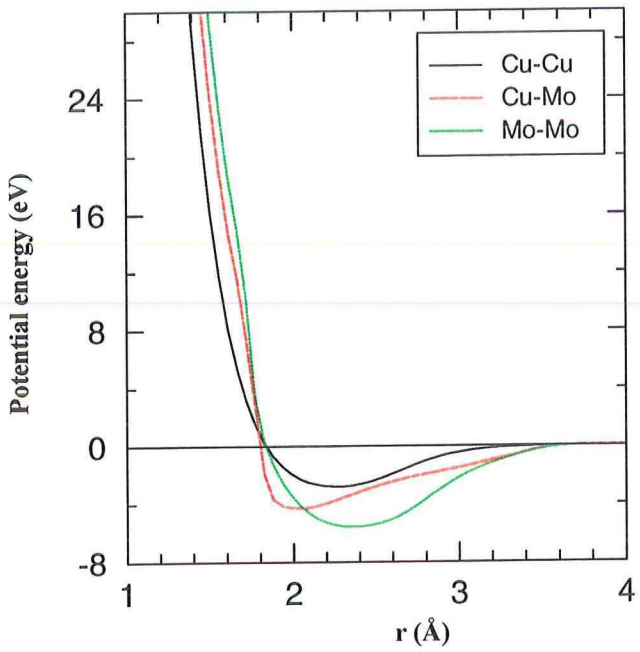

Fig. 1. Potential energy of a pair of Cu atoms, a Cu and a Mo atom and two Mo atoms against the distance between the atoms. Note that this is the interaction between two atoms and not a complete crystal.

Mo-Mo interaction

Our group has used the EAM Mo-Mo potential for several years, hence it is quite elaborately tested. Although a more recent article [8] indicates that this method is less reliable for transition metals because there is no angular dependence in the EAM functions, our group has found no strange phenomena for molybdenum that are directly related to this remark. Transition metals have partial filling of the *d* bands which implies an angular character to the interactions, but the EAM potentials have spherically symmetric interactions. The details of the used Mo-Mo interaction potential have been described by Klaver [7], the choice for the analytic functions for the embedding function, the pair potential and the electron density is based on work by of Johnson and Oh [13]. Here we will give only the highlights of this potential function.

The electron density, the embedding function and the pair potential have the following analytic expressions for a number of bcc metals:

$$f(r) = f_e \left(\frac{r_{1e}}{r} \right)^{\beta}, \tag{14}$$

$$F(\rho) = -(E_c - E_v^{uf})\left(1 - \ln\left(\frac{\rho}{\rho_e}\right)^m\right)\left(\frac{\rho}{\rho_e}\right)^m, \tag{15}$$

$$\phi(r) = K_3\left(\frac{r}{r_{1e}} - 1\right)^3 + K_2\left(\frac{r}{r_{1e}} - 1\right)^2 + K_1\left(\frac{r}{r_{1e}} - 1\right) + K_0 \tag{16}$$

in which m, K_0, K_1, K_2 and K_3 have values calculated from five expressions [7, 13] that relate these parameters to experimental values such as cohesive energy etc. These parameters and the used experimental values are given in Table I. Just as for the Cu-Cu potential function a few alterations are made: [1st] a slight alteration of the embedding function near $\rho = 0$ to prevent a singularity in the derivative of the embedding function; [2nd] the number of interactions is limited due to changes in the electron density and the pair potential for large distances (cut off distance is 3.80 Å); [3rd] the pair potential is stiffened for 1.59 Å $< r <$ 2.70 Å and for $r \leq$ 1.59 Å the EAM function is replaced by a Screened Coulomb pair potential (Firsov-Molière). The last alteration has been made by decreasing the electron density to zero and connecting the stiffened EAM potential to the Screened Coulomb potential near this distance. In Fig. 1 the potential function of two molybdenum atoms is shown. A slight shoulder in this function is seen, this is due to necessary replacement of the EAM potential function for a pair potential at high energies.
See [7] for a check of accuracy of the program and reproduction the input parameters.

Cu-Mo interaction
This interaction has also been shaped with the embedded-atom method because many parameters are already known for both materials for this method. The total potential energy for this method is

$$U = \sum_i^{Cu} F_i(\rho_{Cu-Mo}) + \sum_j^{Mo} F_j(\rho_{Cu-Mo}) + \tfrac{1}{2}\sum_{all\ pairs}\phi_{Cu-Mo}(r) \tag{17}$$

in which F_i, F_j are the embedding functions of the copper atoms respectively the molybdenum atoms. The embedding functions have the analytic forms as mentioned before and the same parameters are used except when mentioned otherwise. For the electron density that a certain atom experiences is taken

$$\rho_{Cu-Mo} = \sum_i^{Cu} f_i + \sum_j^{Mo} f_j \tag{18}$$

in which f_i, f_j are the contribution to the electron density of this atom of respectively copper and molybdenum atoms; the analytic form is described in respectively the Cu-Cu and Mo-Mo interaction. The parameter f_e in both these equations needs to be scaled for this interaction (this time this value does not disappear in the ratio of ρ). This has been done by fitting a potential function for a hypothetical b.c.c. compound $Cu_{50}Mo_{50}$ so that the difference in total energy at 0 K is +0.27 eV (heat of formation, see [17]) comparing this compound with the summed total energy of a copper b.c.c. crystal and a b.c.c. molybdenum crystal. Table I gives the values for f_e. The pair potential has been formed after the pair potential of the EAM Cu-Cu interaction:

$$\phi_{Cu-Mo}(r) = \phi_e e^{-\gamma\left(\frac{r}{r_{1e}} - 1\right)} \tag{19}$$

in which r_{1e} is the first neighbour equilibrium distance of the hypothetical compound (r_{1e} = 2.64 Å), γ *is* chosen as in the Cu-Cu interaction and a value for ϕ_e is found by connecting this

pair potential to a Screened Coulomb pair potential (Firsov-Molière) for small distances (r ≤ Å) (the embedding function was taken zero). The number of interactions is automatically limited due to the use of the already adjusted embedding functions for the potential (see Cu-Cu and Mo-Mo interaction); the EAM pair potential is also adjusted as in the Cu-Cu interaction with a cut off distance of 5.02 Å. Fig. 1 shows the interaction potential for a Cu and Mo atom.

The energy difference between one and two monolayers of Cu deposited nominally on the Mo substrate in the simulations resembles very well with the work by Paunov and Bauer [18]. Here it is determined that the desorption energy of the first Cu monolayer is 3.53 eV and of the second Cu monolayer is 3.17 eV. The difference is 0.36 eV, this experimental value is the same as the value calculated from the simulations. This result indicates that the Cu-Mo interaction potential works reliably.

Noble gas interactions

About this potential function we can be short: these interactions are formed by the Screened Coulomb pair potential with Molière weight factors and Firsov screening length (see also Cu-Cu interaction). As a result this potential is always repulsive. As shown in Fig. 2 a minimum in the He-metal interaction of a few milli-electronvolts is not modeled. Also cross the He-He and Ar-Ar interaction at a distance of ~3.2 Å. Pair potentials model the high energy, short range interactions correct; the previous two remarks indicate that the long range interactions are less reliable.

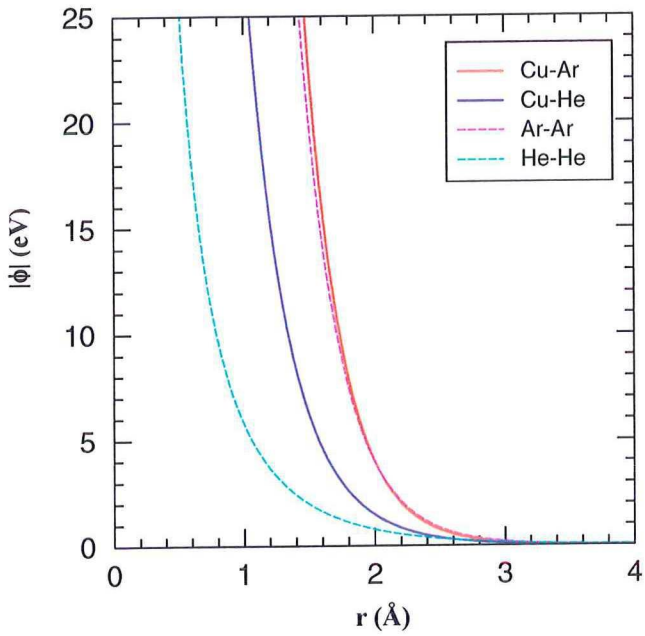

Fig. 2. Potential energy shaped by pair potential part of interaction between Cu and He or Ar, and two He or Ar atoms against the distance between the atoms.

Limitations

As said before the chosen interaction potential is very important for the way the simulated system evolves. The choice of the potential function is bound to the limitations of CPU power

and computing time. Even during the time the simulations for this thesis were performed, the programmes and computers in our group became 1.5 and 2 times respectively faster, yet still the hardware possibilities are the main cause for many limitations in the molecular dynamics. Two other serious limitations are the simulated time and the number of simulated particles in the system.

Short simulation times

The simulated time period ranges from 35 ps to a maximum of 1.1 ns. To give an idea of the real time it takes to perform a simulation with the most used simulated period (~1 ns) and a system of 5500 atoms (20 Å Cu and 14 Å Mo), in the early stage of this research it toke about a month; later on this has been reduced to nine days. The largest simulation of this thesis, a system of 108000 atoms and simulation time of 1.8 ns will take about three months on a supercomputer (Cray) and is not yet finished. The simulated time period is very short (~1 ns) in comparison with the typical 'duration' of an experiment, about 1 s. A consequence of these very short simulation times is that the chance that an atom moves thermally is strongly reduced. Fig. 3 shows the difference between the number of expected 'jumps' of atoms for the experiment and the simulations at 300 K for several thermal processes (with different activation energies). This figure is based on

$$N(Q) = \upsilon_0 t e^{-Q/kT} \tag{20}$$

in which N is the average number of successful jumps of an atom for which an energy Q is required in a period of time t, v_0 is the frequency (a sound estimation is 1.10^{13} oscillations/s) and Q is thus the activation energy of a thermal atomistic process such as bulk diffusion. This equation holds for classic independent quantummechanical oscillators. This is not the case; the merit of Fig. 3 lies in the clear overview why short simulation times limit the number and

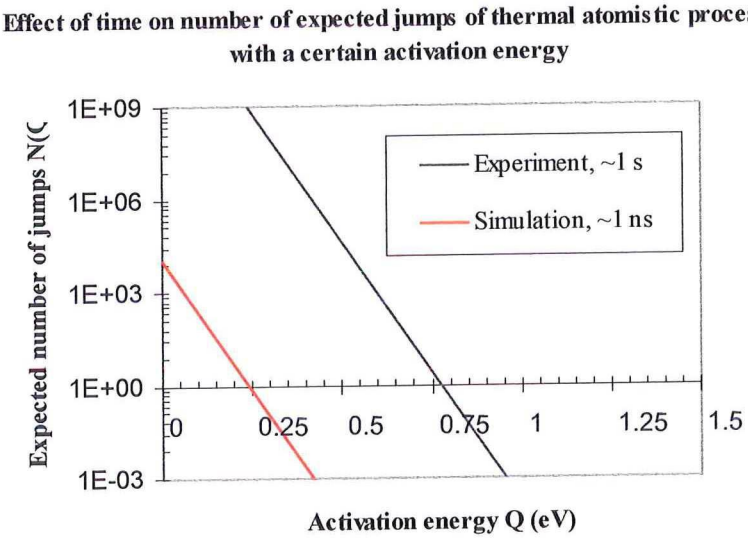

Fig. 3. Effect of time on the number of expected jumps of thermal atomistic processes with a certain activation energy. Black and red lines compare experiment and simulation at same temperature: only processes with very low activation temperatures appear in the simulation.

type of thermal processes that can occur. Processes with low activation energies (0-0.25 eV) can occur in the simulations. Thermal processes that require a higher energy (0.25-0.75 eV) will occur in the experiment; in these short simulations these processes will not be seen (only processes that are sufficiently activated, i.e. $N(Q)>\approx 1$, can be seen in a simulation / experiment). In Ch. 3, third section a method to reduce the consequences of this limitation for these activation energies is given. The simulation of processes with even higher activation energies, such as desorption processes, >1 eV, is not feasible. Only part of the experiment, the He bombardment and decoration of defects is simulated.

Simulation of a system

The size of the used systems is mentioned above, this is very small in comparison with the experiments. Periodic boundaries are used to artificially enlarge the system (in lateral directions). A consequence is that the encountered phenomena are limited in size. The periodic boundaries can influence the growth of the copper films, since the size of the periodicity is determined by the Mo substrate. Another restriction in the use of the periodic boundaries lies in the energy of the impacting atoms in the film. An atom with large implantation energy can cross the periodic boundaries many times and thus the impact can interact with itself.

2.2 Thermal Desorption Spectrometry

Principles

Thermal Desorption Spectrometry (TDS) is an experimental technique in which small inert atoms such as helium atoms are used as probes for defects in thin layers. The apparatus for TDS is schematically shown in Fig. 4. The UHV facility is separated in two chambers; the left chamber is used to grow the thin films with or without ion beam assistance (IBAD) and the right chamber is used for TDS. A TDS experiment is performed in two steps.

First (1), helium ions are implanted in the thin film (these ions become atoms in the film). The helium atoms are mobile at room temperature and can move interstititially through the lattice [5]. Part of the helium atoms will be trapped in the defects of the thin film because the helium experience a local potential energy minimum at monovacancies and vacancy clusters. The most part of the injected helium will escape the thin film through the surface. The energy of the implanted helium ions is of importance; if this energy is too high, the helium will create defects instead of probing the intrinsic defects of the thin film. According to

$$E_{th} = E_d \frac{(M+m)^2}{4Mm} \tag{21}$$

which is based on the maximum energy transfer in a head-on collision of two particles with mass m and M (helium and copper in our case), the threshold energy E_{th} for helium-copper collisions is 89 eV. In this equation E_d is the bulk displacement energy and is taken 19 eV for copper [11]. Below the threshold energy one expects no displacements of copper due to a collision with a helium atom and thus no creation of defects due to the implantation. However, this equation holds only for bulk copper. The threshold energy E_{th} for helium-molybdenum collisions is 250 eV [19].

Second (2), the thin film is heated so the trapped helium atoms desorb from the thin film. At certain temperatures characteristic for the dissociation energy, helium detaches from the

defects by thermal vibrations and escapes through the surface. A mass spectrometer (QMS) can detect the increased number of helium atoms in the chamber. The heating of the sample is linearly in time and the results of mass spectrometer against the temperature ramp forms a collection of peaks called a thermal desorption spectrum. The area of the peak, the shape of the peak and the temperature of the peak maximum give information respectively of the number of defects in the thin film, the type of desorption and the dissociation energy of the helium atoms from the defects which in turn gives information about the type of defect and the number of helium atoms in the defect. Usually a series of spectra is created by variation of a certain parameter, for instance the layer thickness of the deposited film. Examples of series of spectra are given in Sec. 5.1 in which the results of the TDS experiments on the Cu/Mo films are stated.

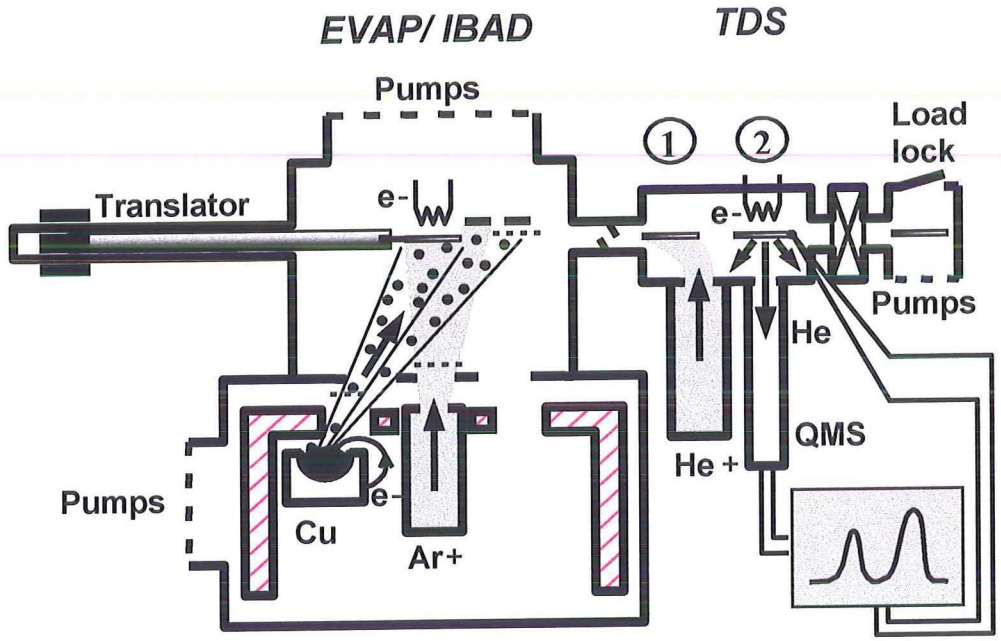

Fig. 4. Schematic reproduction of ultra high vacuum (UHV) apparatus. In this facility thin films can be grown with or without ion beam assistance at different temperatures and analysed with thermal desorption spectrometry. The translator is used to move the sample, the loadlock can be used to change the substrate. The heating is done with electron bombardment. The quadrupole mass spectrometer (QMS) can detect small partial pressures.

Limitations

Interpretation of spectra can be rather complicated for some materials. This is of course the reason to use simulations to aid the interpretation. Especially the trends in the variation of certain parameters can be of assistance in the interpretation. The analysis is indirect, and the number of complex mechanisms that can occur are large. For instance, retrapping in defects with different or same dissociation energy of original trap. A desorption spectrum gives information only about the process that brings helium atoms from their last trapped positions to the surface. In our case the spectra give information about the bombardment of two materials and the spectra of copper have a narrow temperature range [20].

A limitation of a different nature is deterioration of the sensitivity of the quadrapole mass spectrometer; in the latest research fluctuations have been observed and it is possible that this has happened also in earlier measurements (these are used in Ch. 5).

3 L'entrée

In this chapter we will first treat the thin films that were bombarded with helium atoms, followed by an overview of the simulations, and in the third section we will present two solutions for reducing the consequences of two limitations (short simulation time period and system size, see last part of Sec. 2.1) of the simulation method. Some preliminary simulation results without helium bombardment are also shown in this section.

3.1 Starting point: Cu/Mo films

In this section the Cu/Mo films that are used in the simulations of the helium bombardment are introduced. These copper layers are either evaporated or grown with assistance of an argon ion beam on molybdenum (110) substrate. The Cu/Mo films need a short introduction because the evolved microstructure of the films is not obvious. In this thesis we mean by film both the deposited atoms (Cu) and the substrate (Mo). Layer is used if only the deposited atoms are meant. A plane is a layer of a thickness of only one atom usually in the x-y direction. Layers of several thicknesses were used; here we will show the 20 Å Cu layer for this thickness is mostly used. Both the evaporated (Physical Vapor Deposition, in this thesis usually referred to as EVAP) and the layer deposited with ion beam assistance (IBAD) are depicted in Fig. 5. The Cu/Mo layers have been grown by B.S. Bunnik and the first results

Film
Layer
Plane
EVAP
IBAD

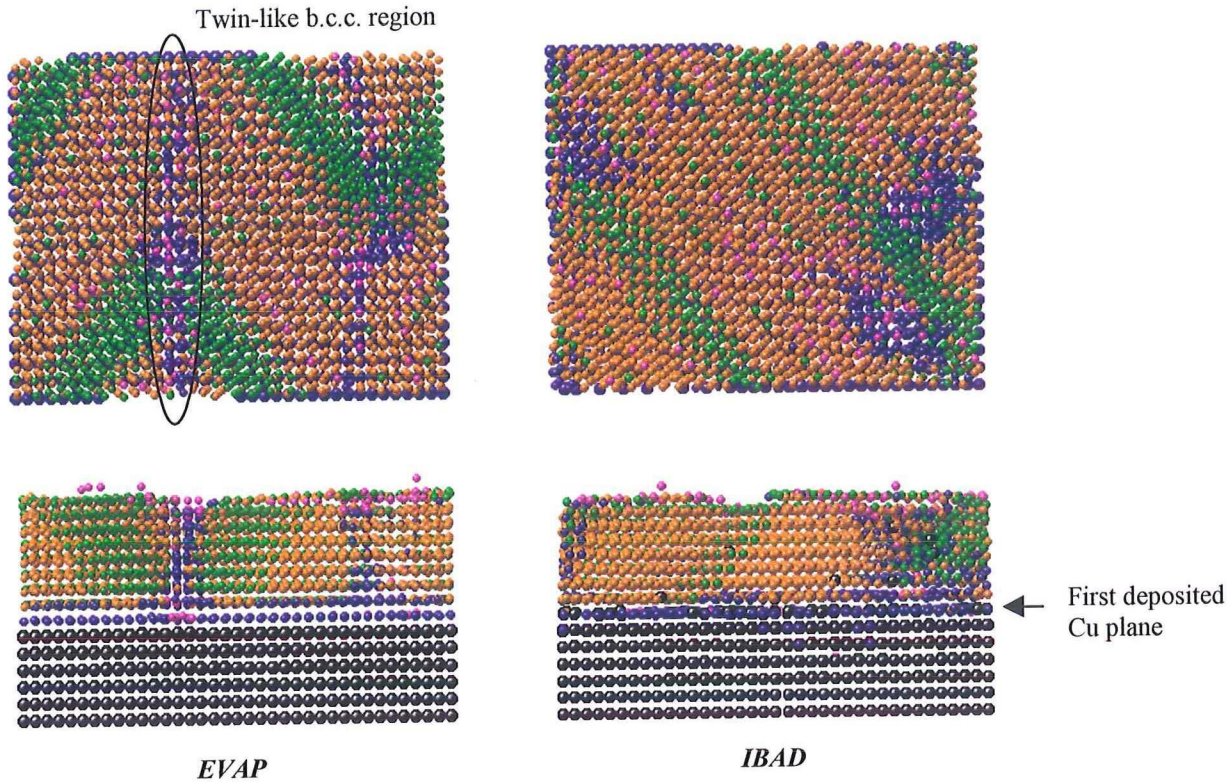

Fig. 5. Topview and sideview of 20 Å evaporated (EVAP) and ion assisted deposited (IBAD) copper layer on molybdenum substrate (colored black). The colors of the copper atoms indicate the local crystallographic geometry: blue = b.c.c., green = f.c.c., orange = h.c.p. and pink = unidentified. The size of the Mo atoms is somewhat large in proportion to the size of the Cu atoms. This underlines the presence of the Mo atoms in the copper layer in the IBAD film. These views show cooled configurations.

have been published [16, 21]. The area of these films is 56.6 × 44.6 Å^2. The molybdenum substrate is 14 Å. In this thesis we number the planes from the bottom to the interface for both materials. In Fig. 5 the Cu atoms are coloured according to the local crystallographic geometry. To improve the analysis of the structure of the grown films, many configurations are rapidly cooled to 0 K. Thus the disturbing effect of the thermal vibrations for example on the structure and potential energy are eliminated. The figure captions indicate whether the shown data is obtained from cooled configurations. In the topviews can be seen clearly that the Cu does not form a simple f.c.c. structure. Instead, one observes a complex structure of alternating f.c.c. and h.c.p. bands, separated by strips with partly a b.c.c. structure. In the EVAP film, twin-like b.c.c. regions develop likely due the mismatch between Cu and Mo. One of these regions is marked in Fig. 5, in these two twin-like regions one would expect the 75 eV helium atoms after decoration, because in these regions the lattice is less ordered. In larger evaporated Cu/Mo systems strips of b.c.c. regions are still spotted, but not in this twin-like set-up, therefore these regions may be a consequence of the system size and less realistic. The sideview of the EVAP film shows that the first deposited Cu plane closely follows the Mo b.c.c.(110) structure. In the IBAD film the interface is less abrupt: the first monolayer grows more irregular, and Cu and Mo intermixing takes place (this effect can be seen in the sideview of the IBAD film): 20% of the Cu and Mo atoms in the interfacial planes end up on other sides of the interface. Only one argon atoms is being encapsulated in this growing film (IBAD), further conclusions about argon concentrations etc. would not be firmly grounded with these statistics. Also interesting is the fact that the growth of both the Cu thin films on the Mo substrate can be distinguished in three regimes (not shown): plane by plane growth for the first monolayer, followed by island growth and after about 10 Å back to the plane by plane mode. In the IBAD layer these modes are less pronounced.

Numbering of planes

One of the mayor differences between the films grown in the experiment and in the simulations is that the evaporation rate is 0.5 or 1 Å/s in the experiment. In the simulations due to the short simulation times this is enhanced to 5.10^9 Å/s. In the experiment the copper layers are deposited at 300 K, in the simulations at 1012 K. The reason for this increase is the same as for bombardment of helium at a higher temperature, see last section of this chapter. In both the experiment and simulations the angle of incidence of the copper beam is 15° off normal (result of the design of the experimental apparatus). The IBAD layers were grown in the simulations under the same conditions of the future experiments: the angle of incidence of the ion beam (Ar^+) is perpendicular to the sample and 15 % of the impacted Ar have a energy of 250 eV instead of the usual 100 eV. The ion to atom ratio was taken 0.1 which is a normal value for ion assisted growth.

3.2 Scope of simulations

In total about 35 simulation runs were performed. The nature of the runs differs: nine long simulations of helium decoration and the reaction of the film hereupon, 19 runs with several goals such as the behaviour of copper atoms at a certain temperature and also 205 configurations were cooled in different runs. The simulations were performed to help interpret the Thermal Desorption Spectrometry experiments. There are only preliminary results form the experiments, only a few parameters are varied, see Ch. 5. The simulation results are used to qualitatively search for an explanation for the experimental results. Often the statistics of

the trapped helium atoms are not elaborate enough to draw firm quantitive conclusions. The results of the simulations are also interesting in itself: the motion of several nanoprocesses can be followed for example diffusion events of the copper, helium trajectories and reactions of the copper on the helium impacts such as replacement collision cascades. So the results of the simulations will be compared with the results of the experiments, but the simulation results will also be mutually compared against different parameters in the runs.
These parameters follow from the TDS experiment but also from the simulations:

- *Implantation energy*: 75 eV and 1000 eV helium bombardments have been performed. The 75 eV He impacts should not be able to create damage in the Cu/Mo thin films contrary to the 1000 eV impacts. For both implantation energies experimental results exist. For the 1000 eV bombardment adjustments had to be made with the thin film, see Sec. 3.3.2.
- *Temperature*: several runs without He bombardement have been performed to establish an overview of the behaviour of the copper atoms, for example the diffusional behaviour. The simulated temperatures are: 300 K, 800 K, 1050 K, 1100 K, 1200 K, 1265 K, 1282 K and 1300 K, see Sec. 3.3.1. The He bombardments have taken place at 300 K and 1200 K. The He implantation in the experiments always takes place at 300 K. The reason to simulate at 1200 K is explained in the next section.
- *Thickness of the Cu layers*: 10 Å, 20 Å, 40 Å and 47 Å Cu layers have been bombarded. Spectra in which the layer thickness is varied are present.
- *Method of deposition*: both an evaporated (EVAP) and an ion beam assisted deposited (IBAD) copper layer are implanted with helium atoms. Experimentally only physical vapor deposited layers have been grown yet, no IBAD layers. The simulations can yield an expectation about the TDS experiments on IBAD layers. Also an ideal f.c.c. copper crystal (no substrate) is simulated to verify some encountered phenomena.

§ 4.1
§ 4.2
§ 4.3
§ 4.3

The exact parameters for all runs are given at the beginning of each section of the next chapter, here only a global overview is presented. A detailed overview of all simulations is also given in the Appendix. The overview in the Appendix is primarily intended for the members of our group to access all data of the simulations. In Ch. 5 the simulation results are compared to the experimental results.
In the experiment only in the neighbourhood of the thin films helium ions become atoms. In this thesis the He ($He/He^{+}/He^{2+}$) are always referred to as atoms. In the helium bombardment experiments the fluence (number of helium ions per area) is usually 2.10^{14} He/cm^2. Due to a overestimation of the measured current by secondary electrons [19] (an estimation is 31%) the fluence is actually ~$1.5.10^{14}$ He/cm^2. In the simulations the value of the fluence that is taken, is somewhat higher: $4.0.10^{14}$ He/cm^2 (100 He per area of the films). We expect with this fluence that trap mutation does not occur yet (this was registered in molybdenum with a fluence of $2.2.10^{15}$ He/cm^2 [19, fluence with the contribution of secondary electrons]). About every 3 ps a helium impacts on the surface of the films for both the experiment and simulations. Note that the areas differ: 1 He atom in 3 ps in 1 cm^2 in experiment and 1 He atom in 3 ps in $2.5.10^{-13}$ cm^2. The flux in the simulations is thus 13 orders larger than in the experiments. In the simulations 100 He impact in first 284 ps in the thin films, the films are simulated another 780 ps after the bombardment for relaxation.

3.3 Reduction of limitations of the simulation method

In this section some preliminary simulation results are shown. A method to reduce the effects of the short simulation period on thermal motion of the atoms is given, supported by several simulations without helium bombardment (Sec. 3.3.1). Also the size of the system is artificially enlarged because a test run shows that the size of the system is insufficient for 1000 eV helium bombardment (Sec. 3.3.2)

3.3.1 Increasing the temperature to reduce the effect of short simulation times

Method to 'accelerate' thermal processes

As explained in Ch. 2, a limitation of the simulations is the short time for atoms to thermally move. A method to reduce this effect is to heighten the temperature of the simulation. Fig. 6 gives an insight in the relation between the time and temperature. It is based on Eq. (20) in Ch. 2 (also the lines at 300 K in the figure are explained here). The figure shows the consequences of the heightening of the temperature of the simulation to 1200 K. The roman numbers in this figure give different areas of comparison between the simulations and the experiments: **I** although the number of expected jumps for one atom in ~1 ns is lower than in the experiment in one second, in both the experiment and simulation the number of jumps is regarded large, and these thermal processes can be seen in both experiment and simulation; **II** in this area of the activation energy the number of expected jumps resemble for experiment and simulation; **III** in the simulations thermal processes with higher activation energies can appear than in the experiments. However, the 372 K line of the experiment shows that at this temperature these processes can also appear in the experiment and this temperature is so low that no interesting desorption processes have already taken place in the second step of the TDS experiment (heating of the sample) (see also

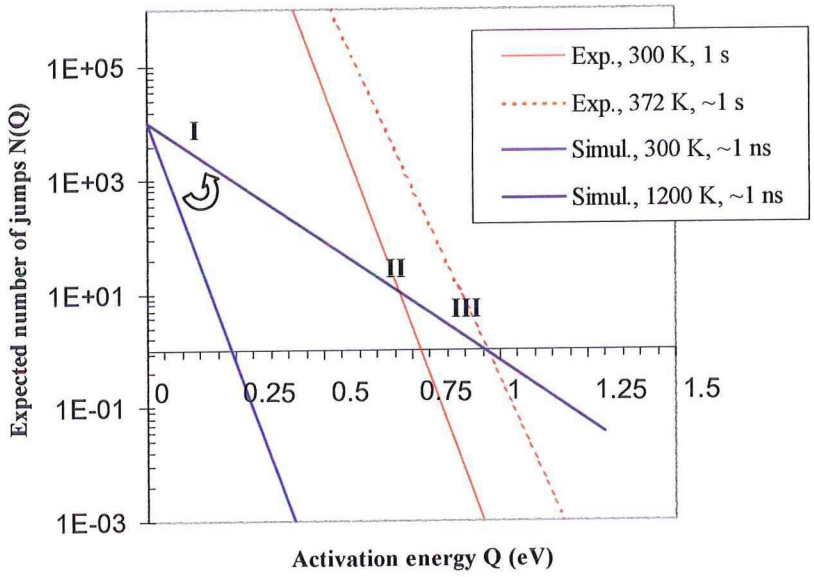

Fig. 6. Effect of time and temperature on average number of expected jumps of atoms in thermal atomistic processes with a certain activation energy. See text for explanation roman numbers. The arrow indicates the course the line follows by increasing the temperature in the simulation.

Fig. 31). In conclusion, the theory seems to predict that 1200 K is a correct temperature to use for the 'acceleration' of thermal processes in the simulations to compare the results more accurately with the results of the experiments at 300 K. If one uses lower temperatures in the simulations, the overall number of expected jumps decreases (see also the arrow in the figure). The reason for taking 1200 K and not a higher temperature becomes clear in the following section where the behaviour of the copper lattice build with this interaction potential is examined (without helium bombardment).

Simulations of behaviour of copper atoms at several temperatures

First an overview of the behaviour of the copper layers at several temperatures is given here, at the end of this section we will return to the behaviour at 1200 K. In molecular dynamics the position of the melting point is influenced by the used interaction potential. Here we are not interested in the exact thermodynamical melting point. The main interest is in the behaviour of the Cu atoms at a certain temperature and whether the behaviour of the atoms at 1200 K is realistic for comparison with the experiments at room temperature. The temperatures used in the simulations are relatively low for molybdenum (compared to the melting point), but 1200 K is quite close to the melting point (1358 K) for copper.

Fig. 7 and views of the displaced atoms in a certain time, Fig. 8, give an idea of the diffusion of the Cu atoms and of the long range order of the lattice. In the Fig. 7 the mean square drift $\left\langle \{r_i(t+\Delta t) - r_i(t)\}^2 \right\rangle_N$ averaged over all N copper atoms is shown for different temperatures, this gives a measure of the overall diffusion of the atoms. With the Einstein equation for diffusion (see for more details [22]) the diffusion coefficient can be

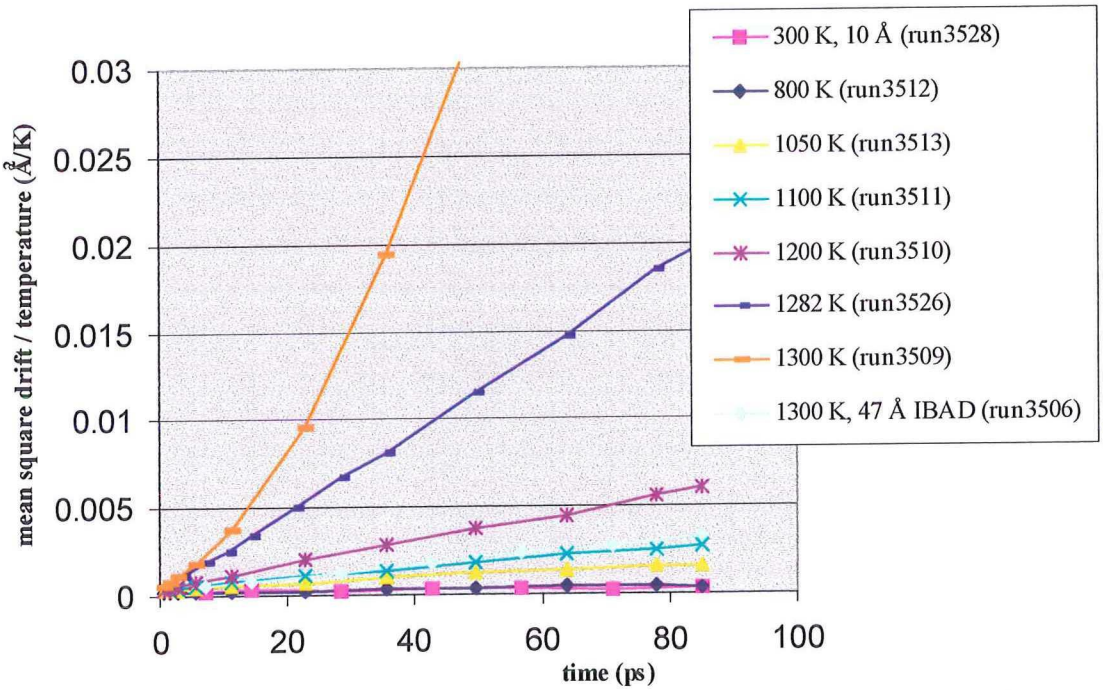

Fig. 7. Mean square drift $<\Delta r^2>$ divided by the temperature against time. Default parameters of simulations are 20 Å copper layer, EVAP, no helium bombardment. Exceptions are mentioned in the legend.

calculated from the mean square drift $<\Delta r^2>$. The diffusion coefficient is proportional to the derivative of $<\Delta r^2>$. However, this equation is valid for stationary isotropic systems and in our case the system is anisotropic (surface diffusion behaves differently in the z-coordinate), there is a gradient (surface and bulk diffusion) and the system is non stationary (mainly at 1300 K for a certain time, the number of randomnized atoms increases). At 300 K and 800 K the figure shows a horizontal line for the diffusion (derivative is nearly zero); this is the usual behaviour of the atoms of a solid: one sees the vibrational movement of an atom around its potential-energy minimum, the so called in-cage movement. Diffusion to different sites of the lattice occurs so little $<\Delta r^2>$ over all the atoms is scarcely heightened, though at 300 K surface diffusion and at 800 K also bulk diffusion is noticed (this involves tens of atoms in 85 ps). In the case of a purely harmonic potential, the in-cage movement of the atoms contributes to $<\Delta r^2>$ proportional to the temperature. To remove this contribution of different temperatures, the drift divided by the temperature is shown in Fig. 7. At higher temperatures $<\Delta r^2>$ increases strongly in time. The number of atoms that participates in both the surface and bulk diffusion increases strongly. The surface diffusion gradually involves more planes. The difference in temperature is only 12 K, but the difference in $<\Delta r^2>$ in Fig. 7 between 1282 K and 1300 K is quite large: at the last temperature the long range order of the lattice is gone (see Fig. 8); the lattice is randomnised except for the first copper plane. This plane has apperently a more tight binding to the molybdenum substrate. Note the difference in $<\Delta r^2>$ of the average Cu atom at 1300 K in a 20 Å and a 47 Å IBAD layer. Displacement views (not shown) clearly show the 47 Å layer is not randomnised at 1300 K. We will return to this phenomena in the next chapter. Striking in this thicker layer is also the large diffusion near the interface (first four planes of Cu) (not shown).

Though the diffusion in the 1200 K run is considerable, the copper layer is still intact at this temperature and it seems a safe temperature to simulate helium impacts. Fig. 9 shows that the surface diffusion contributes mainly to the $<\Delta r^2>$ of the copper layer at 1200 K.

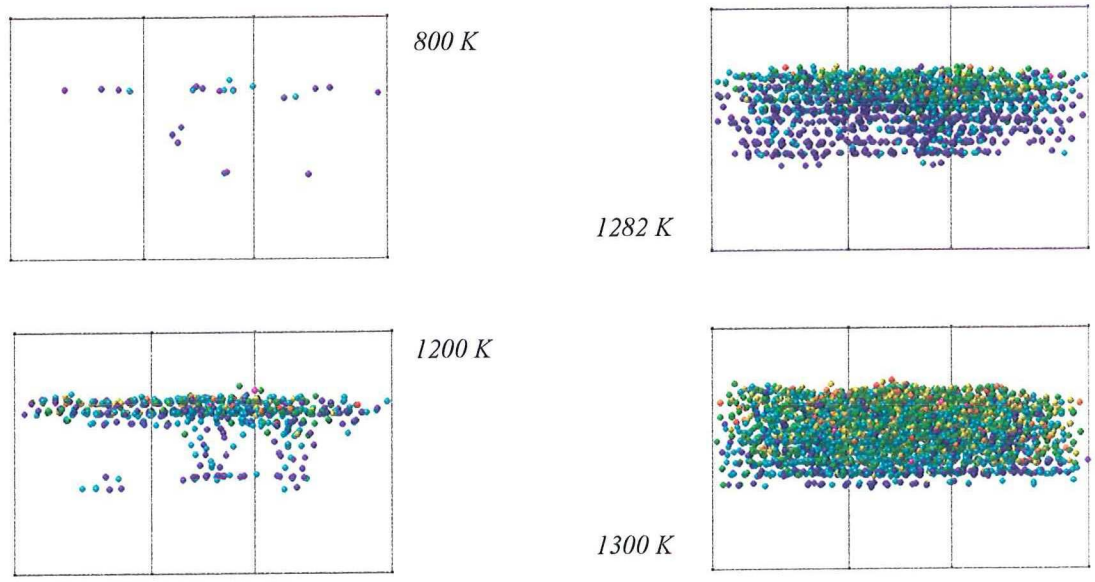

Fig. 8. View of Cu atoms that have moved more than 1.88 Å in 85 ps at different temperatures. Molybdenum substrate and other Cu atoms that have moved less are not depicted. No helium bombardment. Atoms are colored warmer as the displacement of the atoms increases.

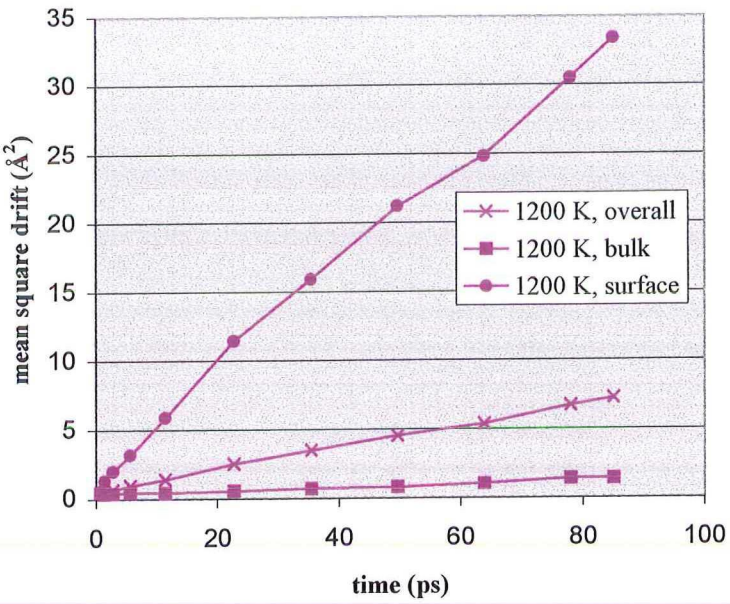

Fig. 9. Contribution to the mean square drift $<\Delta r^2>$ of the surface, bulk and of the complete 20 Å copper layer against time at 1200 K.

3.3.2 Increasing the system to bombard with 1000 eV helium atoms

A test run is performed to explore the impacts of 1000 eV helium atoms. The question is whether the size of the used system (both lateral and in the z-coordinate) is large enough to realistically simulate the 1000 eV He impacts. The thin film of this run (run number is 3503) is a 47 Å copper layer on a 14 Å molybdenum substrate with an area of 57 × 45 Å^2. Fig. 10 shows the absolute and relative trajectory of the first impacted helium atom in the x and y direction. This helium atom passes five times a periodic boundary. The He atom that remains in the film crosses even 10 times the periodic boundaries. An unrealistic consequence of the frequent crossing of the periodic boundaries can be that the impact interacts with itself for example in the distribution of the heat of the impact.
Another problem with this run is the large number of He atoms that pass through the Cu/Mo film. The transmission is 48% of the impacted helium atoms. Only one helium atom remains in the film (2%). In Fig. 14 the z-coordinate against time is given for several 1000 eV helium impacts in a much thicker film. This figure shows that the penetration of a helium atom in the film is very deep before returning to a higher z-coordinate in the thin film. In the thin film of run 3503 helium atoms that trap are lost because the film is not thick enough to meet that first penetration. Another unrealistic feature in this run is the sputtering of one molybdenum atom of the substrate at the bottom of the box.

The large film of run 3524 (1000 eV, 1200 K) was build to avoid the problems of run 3503. The impact interacting with itself is prevented by enlargement of the system in the x and y direction as shown in Fig. 11. This film exists of six films of normal areas (the new area is 113 × 134 Å^2). The periodicity in the x, y direction is therefore enlarged though the film at the starting configuration is essentially the same as in run 3503. Evolving in time the periodicity

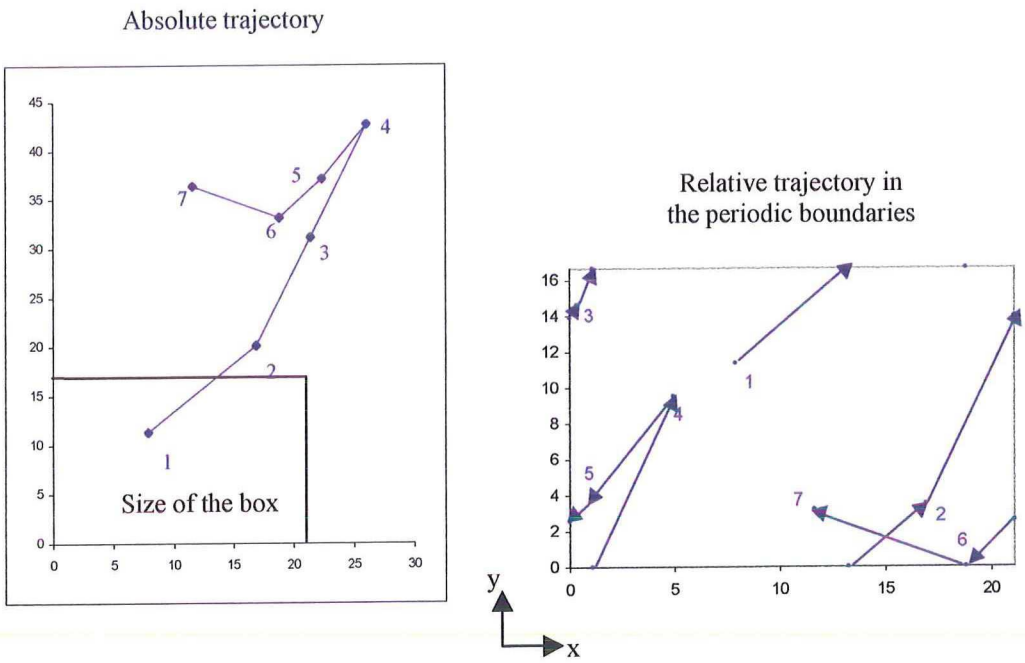

Fig. 10. Absolute and relative trajectory of first He atom impacted with 1000 eV in a 47 Å thick copper layer on a molybdenum substrate. The units are in simulation units: 1 unit = 2.684 Å. The blue lines connect the seven known values of the trajectory of the He atom but this is not the real trajectory.

of first six lattices will be destroyed and periodicity will only prevail over this large area of six films. The substrate is enlarged to decrease the transmission: 66 Å molybdenum instead of usual 14 Å. TRIM simulation of a system with 40 Å copper on 60 Å molybdenum gives a transmission of 32% which is a reasonable diminution with respect to the transmission in the previous system. The choice of the thickness of the substrate is a narrow line between the

number of atoms in the system and the diminished transmission due to thicker substrate, because the time a simulation takes is linear with the number of atoms in the system. The number of atoms for the enlarged system is already about 109000 atoms and will take about three months (simulated time period ~1.8 ns) on a supercomputer (Cray T-3E). This run is not yet finished. At the time this run was started the larger systems mentioned in Sec. 3.1 were not yet grown, therefore this artificial enlargement is used. If the 1000 eV simulations are proceeded, the use of these larger systems is recommended because these films are more realistic; they do not have the repetition of microstructure the presently used system has.

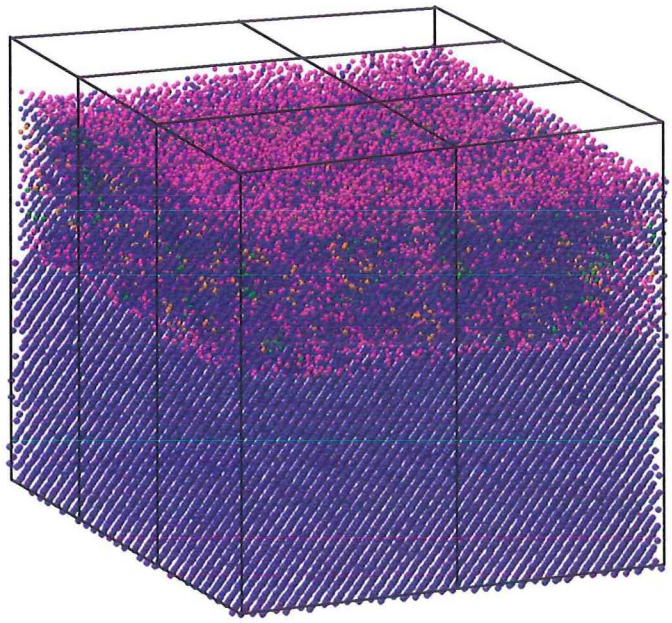

Fig. 11. Illustration of the enlargement of the system to bombard with 1000 eV helium atoms. The configuration at 1200 K at 125 ps is colored according to the local crystallo-graphic geometry: blue = b.c.c., green = f.c.c., orange = h.c.p. and pink = unidentified.

4 Results of helium bombardment simulations

In this chapter information about the helium bombardment in the simulations for different parameters (see for this approach of the simulation results Sec. 2.2) is gathered. In the next chapter this information is used to aid the interpretation of the experimental results. The first section goes into the differences and similarities of helium impacts with different implantation energies. Influence of the temperature is treated in Sec. 4.2. The third section deals with the effects of different thicknesses of the copper layers and the differences in the evaporated and ion assisted grown thin films. Variation in these parameters: energy of He, temperature and thickness of layer give quite different outcomes. In this research unexpected phenomena have been encountered. It is necessary to understand these phenomena more profoundly before the results of the simulations can be used for interpretation of the TDS experiments. We will usually describe these striking phenomena before the behaviour of the helium atoms is characterized.

4.1 Influence of the implantation energy

Introduction

The runs that are most important for this section are given in Table 2; at the end of the section numerical results of the He bombardment such as backscattering and the sputtering yield are shown for the same runs (Table 3).

Table 2. Simulations of 75 eV and 1000 eV He bombardment. The notation of the 1000 eV run indicates the enlargement in both lateral directions and z-coordinate as explained in Sec. 3.3.2.

Implantation energy	*300 K*		*1200 K*
75 eV	Ideal Cu (111) film, 100 He in 284 ps, 780 ps relaxation	20 Å, EVAP, 100 He in 284 ps, 780 ps relaxation	20 Å, EVAP, 100 He in 284 ps, 780 ps relaxation
1000 eV			(40 Å Cu + 66 Å Mo)×6, EVAP, 22 He in 127 ps

Both runs at 300 K are added to the discussion in this section to dismiss the influence of temperature and lattice. Striking in Table 2 is that the two films used in the simulations that can be compared qua implantation energy have a different layer thickness and also the number of impacted He atoms in the 1000 eV run is still much smaller than in the 75 eV run (this run is not yet finished). The area of the 1000 eV run is six times larger than the usual film size (see also Sec. 3.3). These combined facts result in a very low fluence (the number of impacted He atoms per area of the film) for the 1000 eV run, namely $1.4.10^{13}$ He/cm^2. To compare directly the overall results of the He bombardment, the same fluence is necessary for both runs. At this fluence in the 75 eV run only just four He atoms have impacted. Therefore, the statistics of the trapping heliums for this comparison are just too poor to draw conclusions. As already mentioned (see Sec. 3.2), the total fluence for the 75 eV runs is $4.0.10^{14}$ He/cm^2. The simulated time in the 1000 eV run is still nine times shorter than in the 75 eV run so thermal processes have had less chance to appear.

75 eV helium impacts create defects

As announced we will start with a description of one of the unexpected phenomena. Our expectation was according to the theory in Sec. 2.2. Helium atoms with an implantation energy of 1000 eV create damage in the thin films. An implantation energy of 75 eV is below the threshold given by the theory of binary collisions, Eq. (21), and therefore, He atoms with an implantation energy of 75 eV should not be able to displace bulk copper atoms. This is a important starting point of the TDS experiments.

In Fig. 12 the total displacement of the bombarded thin films is illustrated for all runs of this section. Only atoms that have moved a considerable distance between the start and end of bombardment are displayed. The criterion for large displacement is 1.88 Å. This value works in practice well to recognize the chains of displacements at low temperature caused by 75 eV He. This value is also close enough to the first neighbour distance (2.59 Å for ideal f.c.c. copper at 300 K) to secure that only large movements of the copper atoms are shown. Before interpreting this figure, knowledge is needed of the diffusion of copper atoms at 300 K and 1200 K, because it

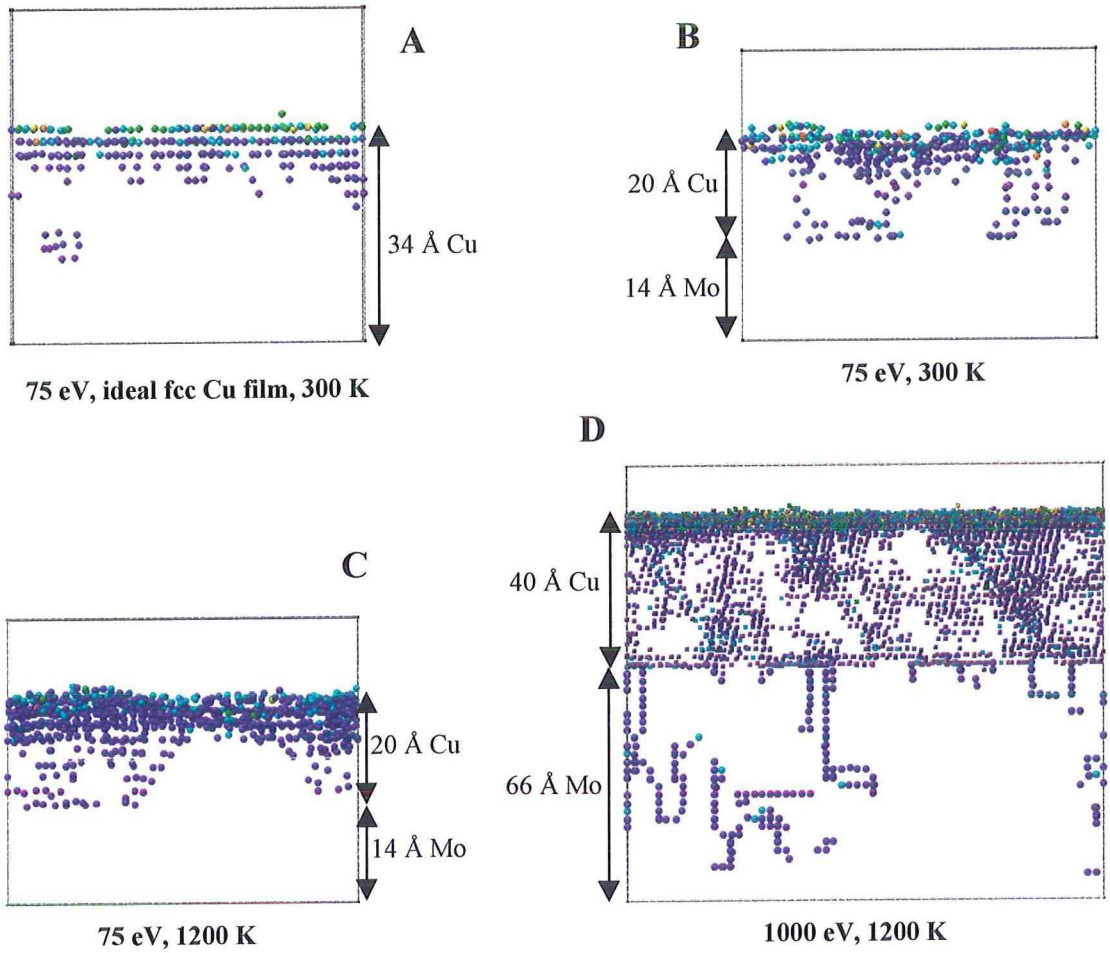

Fig. 12. Overview of copper and molybdenum atoms in thin films implanted with 1000 eV and 75 eV He atoms with at 300 K and 1200 K that have moved more than 1.88 Å during implantation. The fluence in picture A and B is $4.0.10^{14}$ He/cm^2, and in picture C and D ~$1.4.10^{13}$ He/cm^2. The fluence in C is the same as in D for direct comparison. The Mo and Cu atoms are colored warmer as the displacement of the atoms increases. See text for interpretation.

is necessary to know whether the shown displacement is a result of diffusion or due to the impact of the helium atoms. The diffusion of the copper atoms has been treated more elaborately in the previous chapter (Sec. 3.3).
Especially a marginal note has to be placed by picture D of the figure. Here suffice it to say that the shown displacement of the copper atoms of the 1000 eV run does not surpass the displacement by normal diffusion at 1200 K in this 40 Å layer. Therefore, one cannot conclude that the shown displacement of the copper atoms is due to the 1000 eV impacts of helium atoms, because the normal diffusion at 1200 K is so high that the displacements caused by impacts cannot be singled out. However, one can see in picture D of Fig. 12 that many molybdenum atoms are relocated at a considerable depth in the thin film (a depth profile is also shown in this section). This is according to the binary collision theory that 1000 eV He atoms can displace copper and molybdenum atoms. We will return to this point later. The interpretation of the other pictures A, B, C in Fig. 12 is less ambiguous: the shown displacement (due to diffusion and He impacts) is much larger than the displacement by diffusion only in the 20 Å layer at the simulated temperatures. For the 75 eV run at 1200 K (picture C) nearly five times as much copper atoms are relocated by the helium impacts and diffusion than by diffusion only (not shown in figure) in the same space of time. At 300 K the diffusion is limited to a few surface atoms. Therefore, the displacement shown in A en B is nearly completely due to the 75 eV helium impacts. Now an indication of the displacement due to He impacts is established, we return to the figure.
To start again with picture D, the expected damage can especially be observed in the displacement of the molybdenum atoms. The fluence in picture C is taken the same as in D for comparison. Picture C shows unexpected displacement of the copper atoms, especially bulk atoms have also been relocated. This is in contradiction with the predictions made by the binary collision theory. In this thesis bulk is used from ~13 Å below the surface (5 planes deep). For a 20 Å Cu layer on Mo substrate this is however not really bulk since the interface is near. Picture B shows also 75 eV impacts, only at a low temperature. Again bulk displacement is noticed by subthreshold impacts and now this displacement can no longer be an effect of the temperature. In picture A the influence of our grown films is also dismissed as a cause for the bulk displacement of copper atoms, since here an ideal f.c.c. copper lattice was bombarded with 75 eV helium atoms at 300 K (this film had no defects at the start of the simulation) and again bulk atoms have been displaced. In conclusion, in our simulations 75 eV helium impacts can evidently displace copper bulk and surface atoms. This is contradictory to the starting point of the TDS experiments.
A last remark about this figure has to be made because the shown fluence of picture A and B is larger than the fluence in picture C and D. At 300 K at this range of the fluence an increase of the fluence does not enlarge the displacement of the Cu atoms per 75 eV He impact in time. See also Fig. 22.

These results are supported by simulations by Colla et al [23] in which displacement in Cu is found for subthreshold recoil energies (even for 1 eV) by an 1000 eV Cu impact. Here a tight binding potential for Cu is used. This feature is attributed to the spike existing in the system after impact. Though Cu atoms are found in spike in the bombardment at 300 K, later in this research it became clear that it is not likely that the existence of spikes is the main driving force of the displacements in our simulations.

The next question that arises is, what are the consequences of these displacements of Cu atoms by 75 eV He atoms. The answer is that the helium atoms create space in the lattice by displacements of copper atoms and usually trap in this space. We will later show examples of this mechanism (Sec. 4.2). A helium atom is trapped if the atom resides after bombardment at a substitutional lattice site. Fig. 13 shows an example of this trapping. In this figure a bulk plane of the 34 Å ideal Cu film before and after 75 eV He implantation at 300 K is displayed. The impacted helium atoms (nine helium atoms are shown in this plane, they are colored pink in this figure) take the place of an copper atom: they create monovacancies and divacancies. Two divacancies, single en double filled by helium atoms, and seven monovacancies are shown. Thus surprisingly, 75 eV helium atoms can create point defects in the lattice of our thin films, even at low temperature in an ideal f.c.c. copper thin film.

Trapping

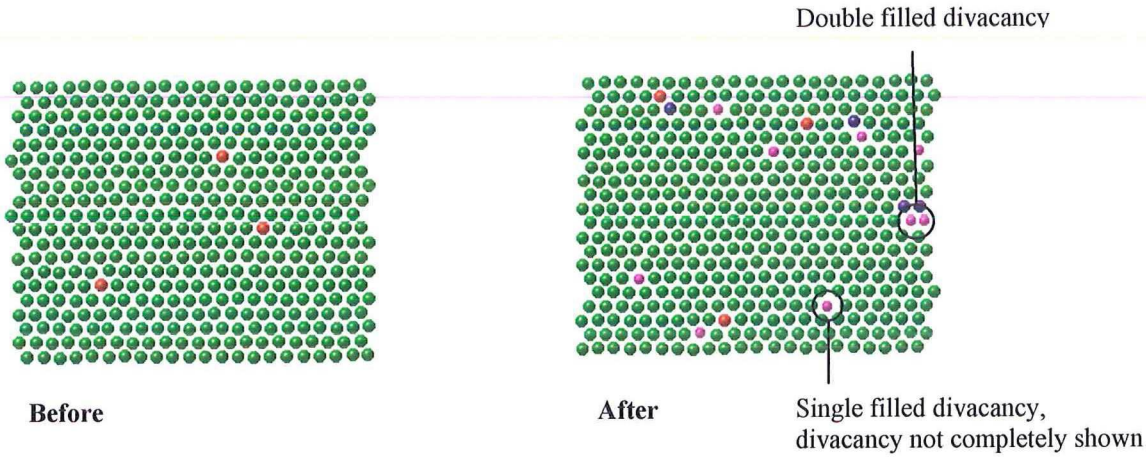

Fig. 13. Bulk plane in ideal f.c.c. copper film before and after He implantation at 300 K. Smaller atoms represent helium atoms (all He atoms are colored pink here) Colors indicate local crystallographic geometry: green = f.c.c., red = h.c.p., blue = b.c.c. and pink = unidentified.

1000 eV bombardment

In this section we will further explore the results of the 1000 eV simulation. The 75 eV runs will be treated more elaborately in the following sections. Fig. 14 and 15 give projections of the trajectories of the helium impacts in this run. In Fig. 14 the z-coordinates of the He atoms are plotted against time. Every 6 ps a new He atom enters the film. The He atoms that hit the surface at 17, 23, 57, 85, 91 and 113 ps pas through the film. Note the difference in movement between the He atoms trapped in the copper layers and in the molybdenum layers. If one looks at the sites of the helium in the lattice after bombardment (not shown), it turns out that the three helium atoms that remain in the molybdenum substrate move interstitially. The other three He atoms, in the copper layer, are trapped in two monovacancies and one divacancy. The type of a vacancy (whether the vacancy is a mono- or a divacancy) is sometimes difficult to estimate at high temperatures, because especially in the b.c.c. twinlike areas there much space and less order in the lattice. However, these He atoms in the Cu lattice are certainly trapped in a vacancy and do not move interstitially. Fig. 15 gives an overview of the lateral motion of the impacted He atoms. In this figure the absolute trajectories of the He atoms and the repeating periodic

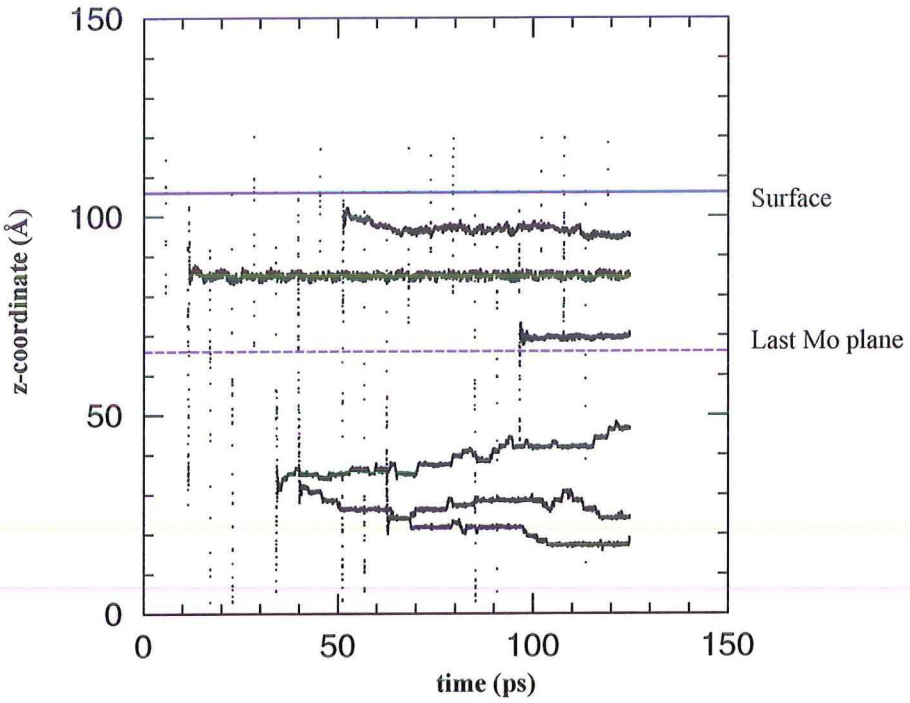

Fig. 14. Projection of the trajectories of the impacted 1000 eV He atoms in the z-coordinate against the time.

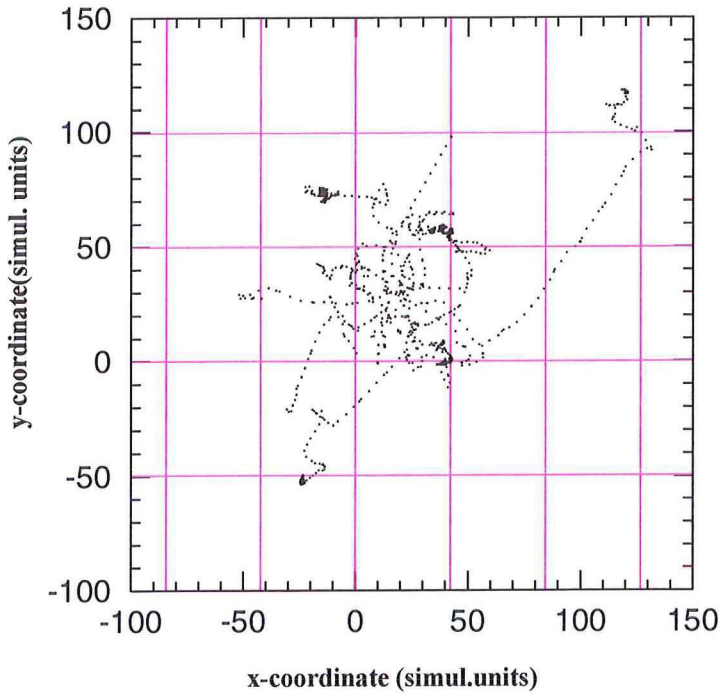

Fig. 15. XY-projection of the 1000 eV He trajectories. The vertical and horizontal lines show the repetition of the periodic boundaries. One simulation unit is 2.684 Å.

boundaries are shown. The number of times a He atom passes a periodic boundary is still considerable compared to run 3503 (see Sec. 3.3.2). The transmission in this run, on the other hand, is down to 29% (Table 3), which is substantial improvement to the transmission in run 3503 (48 %). The percentage of He atoms that remains (trapped or interstitially) in the film is also an indication that the improvement of transmission is important: this is heightened to 29% instead of 2% in run 3503. The predictions of TRIM of the transmission (~31%) resemble strongly with the actual transmission in this run.

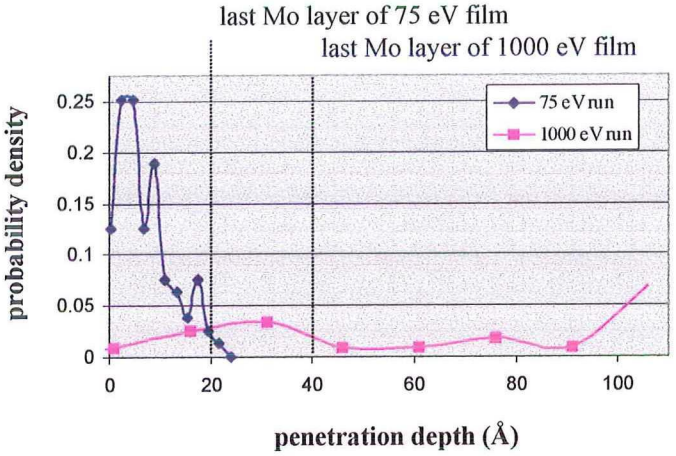

Fig. 16. Fraction of He atoms with 75 eV and 1000 eV implantation energy that penetrated respectively a (20 Å Cu + 14 Å Mo) and (40 Å Cu + 66 Å Mo)×6 thin film to a certain depth at 1200 K.

The depth profile in Fig. 16 illustrates the difference in penetration depth of both energies. The penetration depth of a He atom is defined as the lowest point in the film reached by this atom, usually just after implantation. Fig. 14 shows there is little relation between the penetration depth and the depth of the actual trapping site of the He atom for 1000 eV.

The creation of defects in the Mo substrate is illustrated by Fig. 17. The black atoms represent the trajectory of the 1000 eV He that impacts at 34 ps; the remaining atoms represent the atoms in the lattice that will move a large distance in the next 6 ps. At several points in the trajectory the He atom collides with Mo atoms: a replacement collision sequence (RCS) is the result. For instance

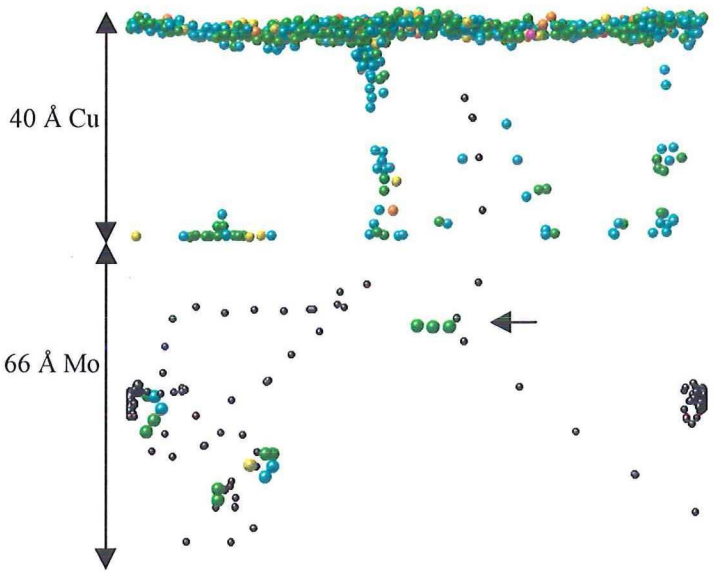

Fig. 17. Overview of atoms that will move more than 1.88 Å in the next 6 ps by diffusion and a 1000 eV He impact (all atoms except the atoms colored black). The black atoms represent the trajectory of that He atom. Note that in a configuration of a certain time, points of a trajectory of several moments are added. See text for explanation of arrow.

at the RCS indicated by an arrow a monovacancy and an interstitial Mo are created (Frenkel pair). The two piles of black atoms are actually, due to the effect of the periodic boundaries, just one collection of points indicating the location where the He atom the rest of the simulation time moves interstitially.

Table 3. General implantation results just after the last implanted helium atom. The deviation in these values increases strongly when the number of implanted helium atoms decreases. Every 3 ps 1 He atom is implanted, except for the 1000 eV, 1200 K run; here the time between implantation is doubled. All values are calculated at the end of the bombardment, except the percentage of thermal leaving (at the end of the total simulation).

	300 K, 75 eV ideal copper	***300 K, 75 eV***	***1200 K, 75 eV***	***1200 K, 1000 eV***
# He in	100	100	100	21
% He left behind in film	22 %	22 %	10 %	29 %
% Thermal leavings	0	0	2	no information
% Backscattering	78 %	78 %	90 %	43 %
% Transmission	0 %	0 %	0 %	29 %
Cu sputtering yield	0.21	0.17	0.21	0.24

4.2 Influence of the temperature

Introduction

Simulations of helium decorations at several temperatures have been performed, these are given in Table 4. In this table the simulations are split in different thicknesses of the copper layers for the behaviour of the Cu layers at several temperatures will prove to be dependent of the layer thickness. The behaviour of the copper layers at several temperatures without He bombardment is discussed in Sec. 3.3.1.

Table 4. Simulations with several thin films at different temperatures. Default parameters of a run are 75 eV implantation energy, EVAP, 100 impacted He in 284 ps, followed by 780 ps relaxation.

Temperature	*Layer thickness of copper →*			
300 K	10 Å	20 Å		
300 K => 1200 K*		20 Å		
1200 K	10 Å	20 Å	40 Å, EVAP, 21 1000 eV He in 125 ps	
1300 K		20 Å		47 Å, IBAD, 24 75 eV He in 78 ps (test run)

*First 284 ps helium bombardment at 300 K, followed by 355 ps relaxation at 1200 K.

The important simulations for this section are the runs with 75 eV helium bombardment in a 20 Å EVAP copper layer on a molybdenum substrate at 300 K and 1200 K. In Table 5 numerical results of these He bombardments are shown. By far most information is gathered about the 20 Å copper layers. The 1300 K runs are witnesses of the evolution of the research. To adjust all (computational) parameters for the long runs, tests were performed with the 47 Å layer (does not randomnise at 1300 K). A result of these tests was that a long run with helium bombardment would take too much time, so less thick layers (the time a simulation takes is linear with the number of atoms in the system) were taken for the long runs. However, as explained in Sec. 3.3.1 the 20 Å copper layer does randomnise at 1300 K without He bombardment (this was only discovered in a long run with He bombardment). Therefore, the 1300 K, 20 Å run with He decoration is less relevant here. Both other temperatures (1200 K and 300 K) were chosen respectively for acceleration of thermal processes such as mobility of atoms (see again Sec. 3.3.1) and to find out the effect of He impacts without phenomena related to the temperature. In this section we will start with the 300 K, 20 Å run, continue with an unexpected phenomenon in the 1200 K, 20 Å run and end with the latest results of the '300 K => 1200 K' run.

Helium decoration at 300 K

At 300 K only a few surface atoms diffuse, thus the mechanisms of 75 eV helium bombardment are not disturbed by thermal processes. Twenty-two of the 100 impacted helium atoms remain in the 20 Å copper layer (Table 5). Neither helium atoms were found in the molybdenum substrate nor move interstitially. At this temperature no helium atoms escaped from the lattice after bombardment. Fig. 18 shows the planes in which the helium atoms are substitionally trapped after the complete run (bombardment and relaxation). We will return later to the 1200 K run. The helium atoms are trapped in 11 monovacancies (all

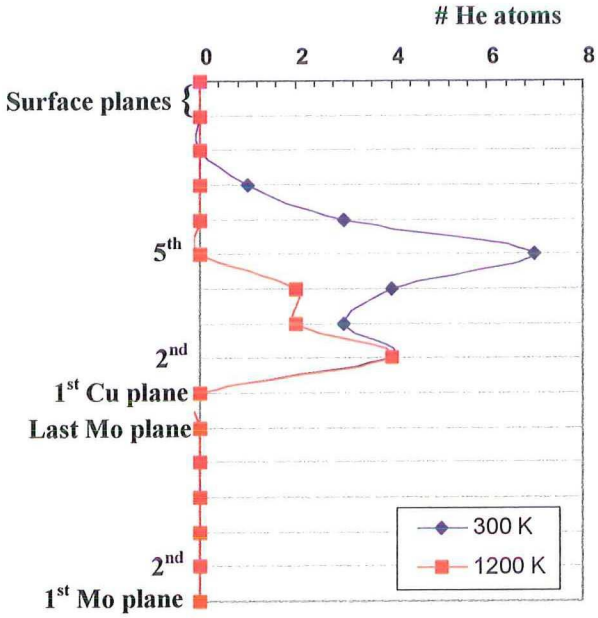

Fig. 18. Number of He atoms per plane in the 20 Å copper layers at 300 K and 1200 K after ~1.1 ns. The connecting lines between the datapoints are given to discern both temperatures, but irrelevant qua physical meaning.

single filled), 4 divacancies (two single and two double filled), and two larger defects: a trivacancy with two helium atoms and a oblong defect with tree He with the space of about four substitutional sites. This large defect is found mainly in the 5th Cu plane. Experimentally, the goal of the decoration with He atoms is to establish a profile of the inherent defects in the grown lattices, but the fact that in the simulations most defects are created by the 75 eV ion beam disturbs this model. However, even in the simulations there are several possibilities the He atoms give information about the lattice: for instance in the impact by displacing Cu atoms in a zone that is less bound, indirectly via a replacement collision sequence that ends in a vacancy, or by diffusion of He via vacancy diffusion indicating less bound regions. For these reasons it is meaningful to determine the type and location (profile) of the He atoms. A rough estimation indicates that fraction of He atoms that trap in a b.c.c. twin-like region (see Sec. 3.1) is larger (~0.4) than the fraction of the b.c.c. regions in the film (~0.2). The original b.c.c. region of the film before bombardment is taken in this calculation (1st, 2nd and surface Cu planes are left out). The difference in fractions indicates it is somewhat easier to displace copper atoms and trap in this b.c.c. region. However, the He atoms displace Cu atoms and trap also in the closepacked regions with more order. Also, dislocations are found in the 20 Å EVAP layer, see Sec. 4.3.2. The defects that exist due to these extra planes are quite recognizable. One helium atom is trapped in such a defect in the 4th Cu plane due to a dislocation. However, even the He atom that resides after impact in this inherent defect has displaced a few Cu atoms to create more space.

A closer look into the individual impacts of the He atoms reveals the mechanism of the displacement of the Cu atoms by the 75 eV He atoms. Fig. 19 shows two examples of this mechanism. Helium atoms create space in the lattice by displacements of Cu atoms and can trap in this space (Frenkel pair). A replacement collision sequence (RCS) of 7 Cu atoms that ends at the surface is the result of the He impact in A after 3 ps. The successive He impacts interact sometimes: in B a RCS of three Cu atoms is shown that will end in a divacancy created by another He earlier in the bombardment. A He is trapped there and this defect decreases to a monovacancy by the RCS. At the start of the RCS a monovacancy is created and the impacting He atom traps there. This He atom escapes the lattice later in the bombardment by two impacts in the neighbourhood. The sequence in B will move forwards; the Cu atoms do not always move in a straight line. In B also a Cu atom is enlarged depicted that diffuses at the surface.

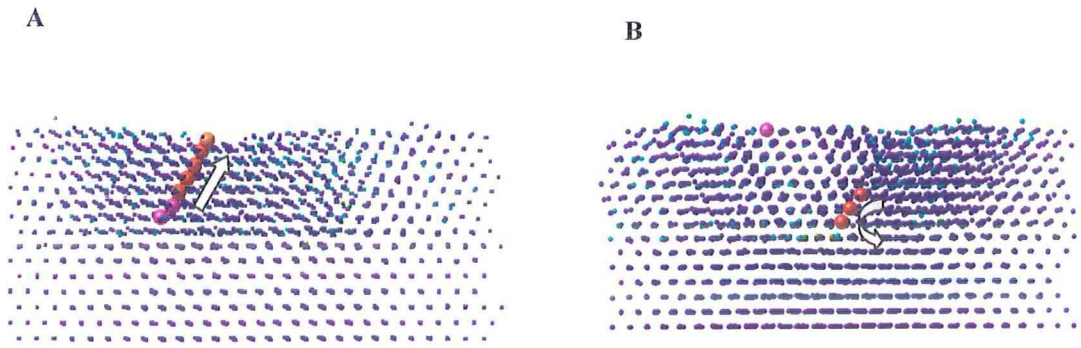

Fig. 19. Examples of replacement collision cascades due to implantation of 75 eV He atoms at 300 K. The atoms are colored warmer as the displacement increases. The Cu atoms that have moved in A, and will move in B more than 1.88 Å in 3 ps are enlarged portrayed. The arrows represent the direction of the RCS.

Helium decoration at 1200 K

Difference in impact of the 75 eV helium atoms between 300 K and 1200 K becomes clear in Fig. 20 in which the number of atoms that move a large distance per impact against the time are given. At 300 K the effect of a helium impact is independent of the previous impacts which is what we expect. On the average about 7 Cu atoms displace per impact. The situation is quite different at 1200 K for the same energy transfer per impact (75 eV) and the same film:

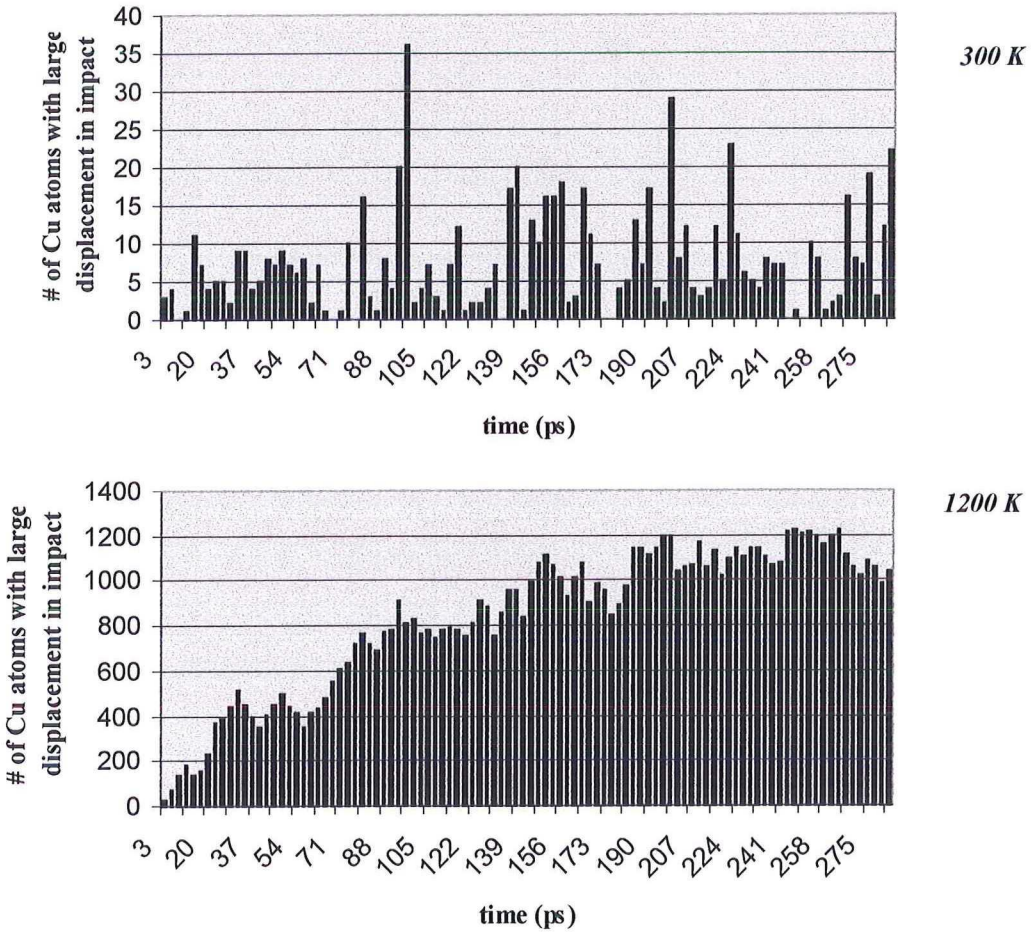

Fig. 20. Number of copper atoms in the 300 K and 1200 K run that have moved more than 1.88 Å in the 3 ps period following each He impact. The energy of the bombarding He atoms is 75 eV and the total fluence is the same: 4.10^{14} He/cm^2. The average displacement (in number of Cu atoms) per 3 ps by diffusion only at 1200 K is subtracted of the figure at the bottom.

as the number of impacts increases, the number of Cu atoms that move over a large distance per impact increases. Note the difference in scaling in the y-axis. The figure of 1200 K is already corrected for the average diffusion (in number of Cu atoms) at 1200 K per 3 ps without He bombardment by subtracting the value 92. Fig. 21 and Fig. 22 shed light on this large number of atoms that move due to the 75 eV ion beam at 1200 K compared to 300 K.

In Fig. 21 the progress of the microstructure in time is given by the number of atoms with a certain local crystallographic geometry for the 20 Å copper layer at both 1200 K and 300 K. The unidentified geometry is given if the local structure does not resemble b.c.c./f.c.c. or h.c.p. It is worthwhile to recapitulate that the film is bombarded with helium atoms during the first 284 ps. The main feature at 1200 K is that the number of Cu atoms with an unidentified geometry increases during the bombardment: the lattice is disordering. The long range order of the lattice (except for the lowest three Cu planes) is gone at 284 ps. The disordering is measured visibly, in a cooled configuration the randomized regions are quite clear. The width of a plane in the z-coordinate for instance, increases considerably in a complete disordered plane. The effect of the bombardment on the structure at 300 K is given as reference; here no structural change occurs as to the extent of the 1200 K run. The randomization is only temporary; after completion of the bombardment the thin film recrystallizes and the number of Cu atoms with an unidentified geometry decreases. Here recrystallization means that the main part of a lattice is ordered again. The number of Cu atoms that are unidentified (from Fig. 21 on the left) is correlated with the number of Cu atoms that displace over a large distance per impact (from Fig. 20) during the bombardment.

The mean potential energy plot (Fig. 22) shows this relaxation quite clearly if one compares the behaviour of the thin film at 1200 K and 1300 K. The bombarded film at 1300 K melts and does not recrystallize. By fitting an exponential ($e^{-t/\tau}$) to the decrease in mean potential energy of the film a value for the relaxation time τ is found and from a rephrase of Eq. (20) in which the average number of successful jumps is taken one in this relaxation time, the activation energy for this process follows: 0.67 eV. In Fig. 22 no relaxation takes place at 300

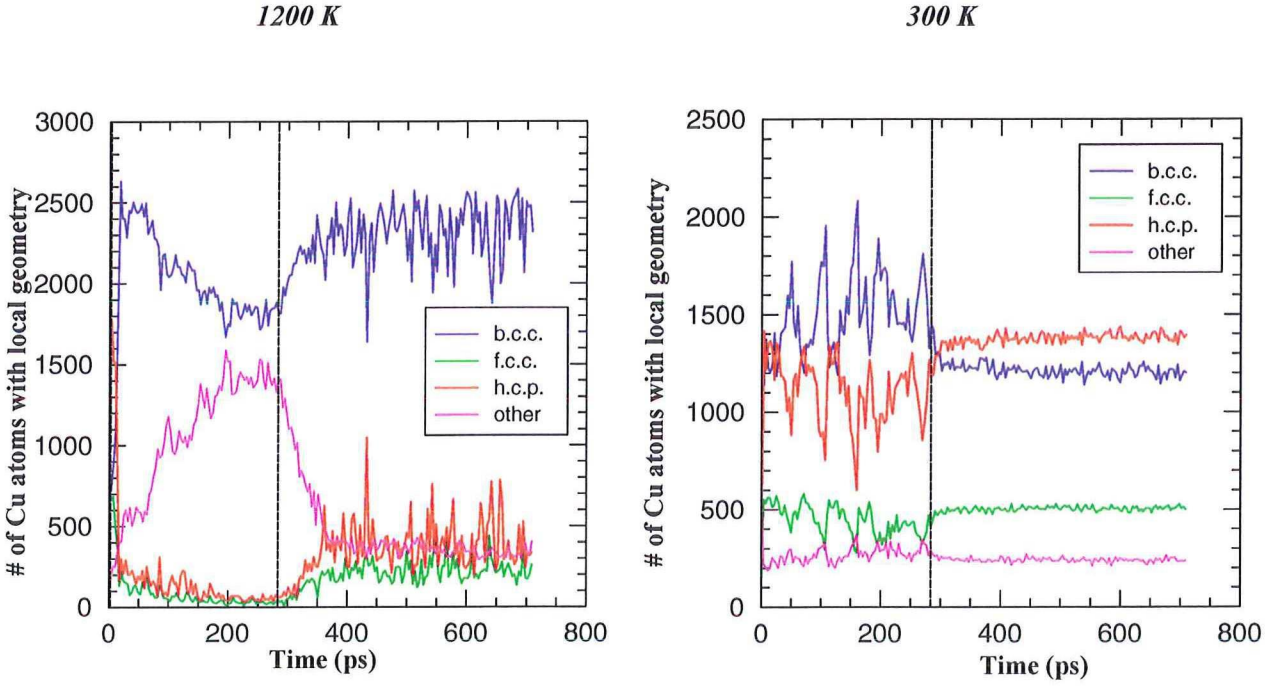

Fig. 21. Number of Cu atoms with a certain local geometry: b.c.c./f.c.c./h.c.p. or unidentified for several configurations in the simulation period. The configurations at 1200 K were cooled. Dashed line indicates the moment of the last 75 eV He impact.

K which is accordingly to our estimation that the short simulation time restricts the processes with higher activation energies. One last remark about Fig. 21, a fast transition from h.c.p. and f.c.c. to namely b.c.c. is seen shortly after the start of the bombardment at 1200 K. This is an effect of the fact that the film at the start of the simulation at 1012 K was. The distribution of the geometry for a 20 Å Cu layer at 1200 K for 85 ps without He bombardment is: ~2700 atoms are coloured b.c.c., ~25 f.c.c., ~70 h.c.p., and ~1050 atoms have an unidentified geometry. The first data point (at 0 ps) is irrelevant.
This ion and high temperature induced temporary randomization is thought unrealistic in the connection to the fact that this run should simulate the experiments at 300 K.

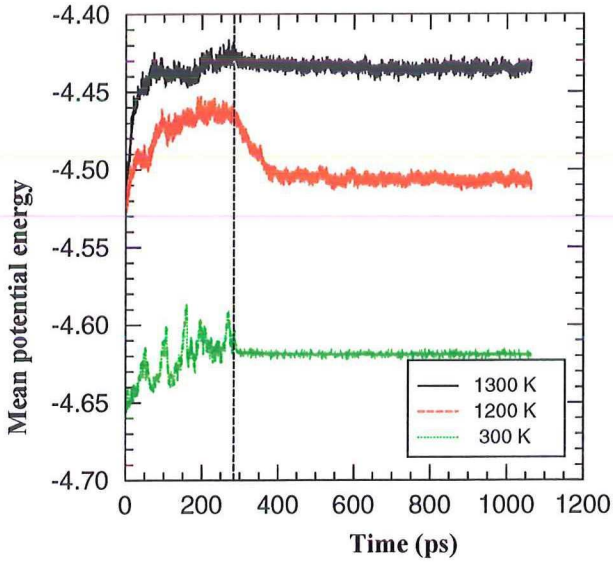

Fig. 22. Mean potential energy of the same Cu/Mo film (20 Å, EVAP layer) against time. Dashed line indicates the moment of the last 75 eV He impact.

In the 1300 K run 21 helium atoms remain in the chaotic thin film (see Table 5); as mentioned before, this film randomizes due to the temperature only and this run shows the behaviour of the He atoms in a Cu layer that is chaotic for most of the simulation and for most planes (except 1st and 2nd Cu plane). At the end of this run the He have clustered in to two very large defects: these two defects spread over four planes (2nd-5th Cu planes), respectively filled with 8 and 13 He atoms. In a randomized Cu layer the He atoms thus tend to cluster in large defects. At 1200 K the situation is more complicated, but since the Cu layer is randomized for a while (although much shorter than in the 1300 K run) we suspect too large defects can develop. After the completion of the bombardment 10 He atoms are present in the Cu layer: two defects (> 3 substitutional sites) filled with 1 He and one large defect filled with 4 He (> 8 sub. sites) in the 2nd and 3rd Cu plane, and four divacancies (rough estimation) filled with 1 He in higher planes. The defects in the 2nd and 3rd planes are not enlarged defects of the dislocations. In the relaxation phase two He atoms escape the Cu layer. In this phase the He also tend to cluster: one defect (> 3 substitutional sites) filled with two He (2nd plane) and one large defect (>> 10 sub. sites) filled with 6 He are present at the end of the simulation. This last large defect spreads over three planes (2nd, 3rd, 4th). This situation is given in Fig.18. The defect filled with two He is part of a dislocation, this is less clear of the large defect.

Helium decoration at 300 K and relaxation at 1200 K

A recent artificial operation in the 300 K run leads to encouraging first results. The 75 eV He bombardment at 300 K is relaxed at 1200 K for 355 ps after completion. This way the temporary randomization is avoided whilst the advantages of the heightened temperature are preserved. A plot of the mean potential energy against the simulation period in Fig. 23. A shows exactly how this was done. After the bombardment at 300 K, a temperature ramp to 1200 K is performed in 7 ps and the mean potential energy strongly increases. After this ramp the temperature is kept at 1200 K. The lattice reacts in essence the same as the film that is also bombarded at 1200 K: the shape of the decrease of the mean potential energy is similar. This is not obvious: the lattice of the '300 K => 1200 K' run is less disordered at the highest point in the plot of the mean potential energy than the 1200 K run just after completion of the bombardment. The similar shape implies that the same process reduces the potential energy. In B of the same figure the planes in which the He atoms reside after the complete run for all three simulations are given. The location of the He at 300 K just after bombardment is the same as after the complete run. After all, the temperature of this run is too low to activate bulk processes for this simulation time. Therefore, in B we also can see the location of the He atoms at the start and end of the relaxation at 1200 K (see arrows) of the '300 K => 1200 K' run. Fourteen He atoms leave the lattice in the relaxation; they depart sometimes in groups at about the same time. Here a group of six He atoms leave at 328 ps via a path to the surface. Vacancy diffusion is in this case the mechanism of motion of the He atoms. Interestingly, the He atoms not only leave the lattice, but also three He atoms relocate to the 2nd Cu plane, deeper in the copper layer. The six He in the 2nd Cu plane reside in two monovacancies (single filled), one divacancy (double filled) and two He in a larger defect (> 5 substitutional sites). The other two He in single filled monovacancies.

To conclude, in the 1200 K run the number of He atoms and their location resemble more to the '300 K => 1200 K' run than in the 300 K run. In the relaxation at 1200 K 14 He have left the film which is considerable. In both runs the second copper plane 'attracts' trapped He.

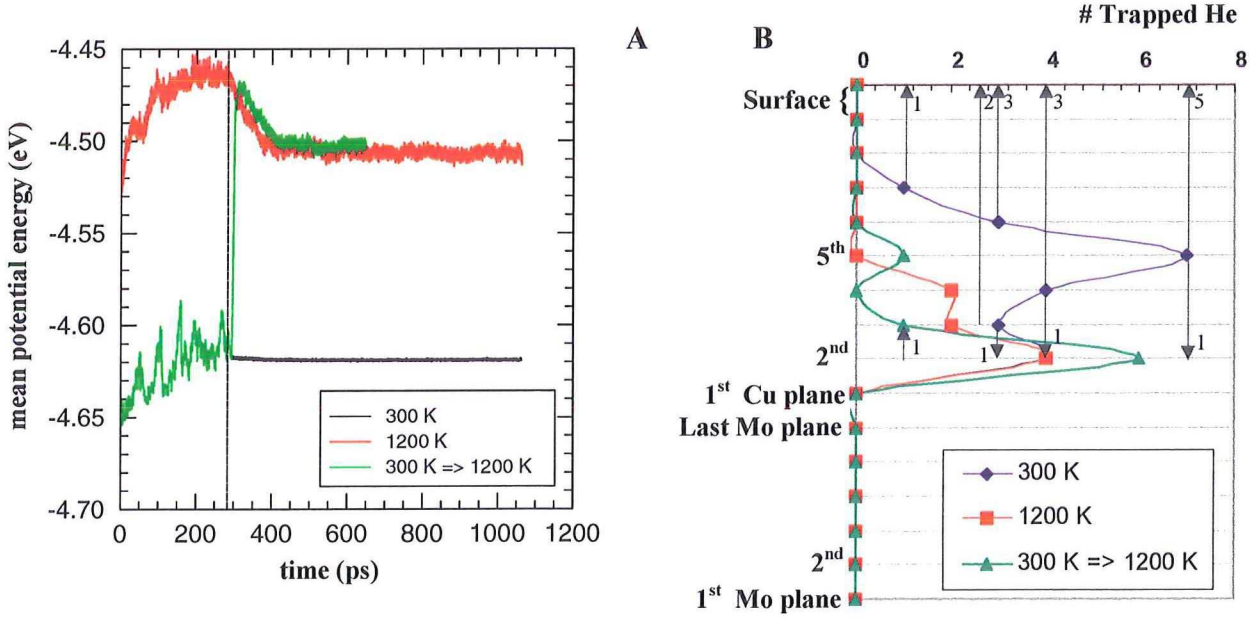

Fig. 23. A. Mean potential energy against time. Dotted line indicates the moment of the last He impact. B. Number of trapped He atoms per plane at the end of the simulations. Arrows indicate the motion of one He atom (figure gives the number of He with the same motion) decorated at 300 K in the relaxation phase at 1200 K.

However, the size and type of the defects in which the He atoms are trapped seem quite large in the 1200 K run, in this the '300 K => 1200 K' run resembles most the 300 K run.

Table 4. General results of the He bombardments. The default parameters of the simulations in this table are 100 75 eV He atoms impacts in a Cu/Mo thin film with a 20 Å evaporated copper layer. After the He bombardment the simulations continued another 780 ps, except the '300 K => 1200 K' run: this run relaxes for 355 ps (and the temperature is heightened to 1200 K). All values are calculated at the end of the bombardment, except the percentage of thermal leavings.

	300 K	***300 K => 1200 K***	***1200 K***	***1300 K***
% He left behind in film	22 %	22 %	10 %	21 %
% Thermal leavings	0 %	14 %	2 %	0 %
% Backscattering	78 %	78 %	90 %	79 %
% Transmission	0 %	0 %	0 %	0 %
Cu sputtering yield	0.17	0.17	0.21	0.13

4.3 Layer influences

Introduction

This section is split in three parts: influence of the thickness of the grown layers, method of growth of the layers (EVAP or IBAD) and we will further explore the consequences of the 75 eV bombardment of an ideal f.c.c. copper(111) crystal surface. For the first part Table 4 can be consulted for the simulations with different thicknesses of the copper layers. The following table (Table 6) shows the runs that are most important for the last two sections. At the end of this section follows as usually a table (Table 7) with numerical results of the He bombardments.

Table 6. Simulations with different 'growth' methods. The thickness difference between the 18 Å IBAD and 20 Å EVAP copper layers is considered to be unimportant. In every run 100 75 eV He atoms have impacted in 284 ps.

Method	*300 K*	*300 K => 1200 K*	*1200 K*	*1300 K*
EVAP	20 Å	20 Å	20 Å	20 Å
IBAD			18 Å	18 Å
Ideal f.c.c. Cu(111) film	34 Å crystal	34 Å crystal		

4.3.1 Film thickness

Thin Cu/Mo film

Beside the already treated 20 Å copper layer, a 10 Å EVAP Cu layer is also decorated with 75 eV helium atoms. Interesting in this Cu/Mo film is the behaviour of the helium atoms near/in the Mo substrate. Fig. 16 shows that a larger part of the helium atoms than in the 20 Å layer should be able to reach the Mo substrate. Also, the complex structure (see Sec.3.1) that is present in thicker layers such as the 20 Å layer has not yet developed in the 10 Å Cu layer. Fig. 24 shows two configurations of this thin layer at 300 K, respectively before and after He bombardment. The configuration on the left shows that the b.c.c. zones are larger than in the 20 Å Cu layer. This can be seen by comparing this configuration and Fig. 13. At 300 K the colouring of the local crystallographic geometry does not yet deviate substantially from the cooled configurations. As shown in Table 4 simulations of 75 eV He bombardment in this layer have been performed at 300 K and 1200 K. In this order we will treat the interesting features and the sites of the He atoms for these runs.

The 75 eV He decoration at 300 K again creates defects in the Cu layer. However, not only copper atoms are displaced by bombardment, even molybdenum atoms are relocated. Two He are trapped in monovacancies in the 5^{th} and 6^{th} Mo plane. Also, two He atoms remain at interstitial sites in the Mo substrate. See Fig. 24, the 4^{th} plane of configuration on the right: one interstitial He can be seen clearly between two Mo planes, the other is less visible in this view. Fig. 25 shows the number of trapped He atoms per plane at the end of the 300 K run. The interstitial He atoms in the Mo substrate are not depicted in this figure. After the bombardment at 300 K there are in total 9 single filled monovacancies, 5 divacancies (3 single filled and 2 double filled with He atoms), 1 single filled trivacancy and 1 defect with two He (~4 sub. sites) in the 10 Å Cu layer. One He atom is present in a vacancy that is connected to an extra row of Cu atoms. Two Mo atoms are present in the first Cu plane (see

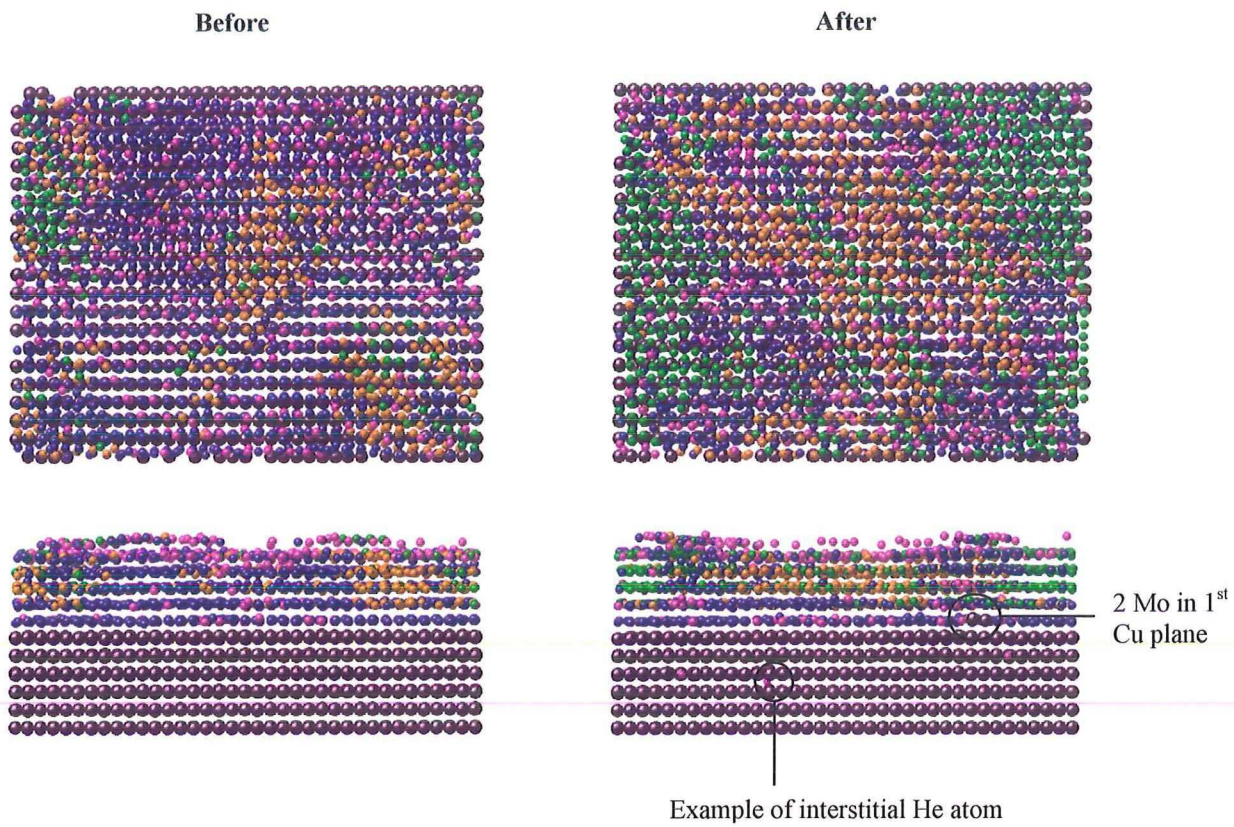

Fig. 24. Topview and sideview of 10 Å EVAP Cu layer on Mo substrate (colored black) at 300 K before and after 75 eV He bombardment. The colors of the copper atoms indicate the local crystallographic geometry: blue = b.c.c., green = f.c.c., orange = h.c.p. and pink = unidentified.

Fig. 24. configuration on the right); these Mo atoms are the effect of two short replacement collision sequences due to the two He that trap at a substitutional Mo site. An interesting feature of this run is that during the bombardment the microstructure seems to change slightly. This can be seen with the use of the local crystallographic geometry. In Fig. 24 two configurations, before and after bombardment, are coloured according to the geometry; the difference in b.c.c. region in the Cu layers is at once clear. In Fig. 26 the local geometry against time is given. A rather sudden transition from b.c.c. to strips of alternating f.c.c. and h.c.p. zones takes place at the end of the bombardment. This is unexpected because the combination of the low temperature and the short simulation time limits the number of processes with higher activation energies. That leaves the bombardment as source for this change, because the bombardment delivers energy to the lattice. The local structure of the 10 Å Cu layer at 300 K without He bombardment is ~1050 atoms b.c.c., ~240 f.c.c., ~500 h.c.p., ~200

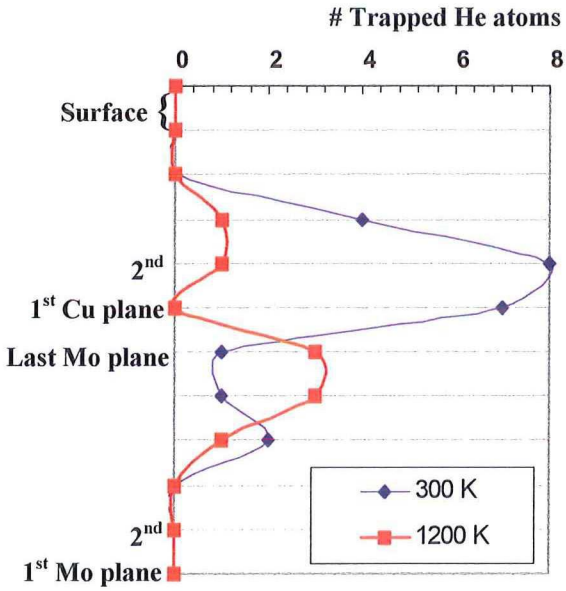

Fig. 25. Number of He atoms per plane in the 10 Å copper layer at 300 K and 1200 K after ~1.1 ns. The connecting lines between the datapoints are given to discern both temperatures, but irrelevant qua physical meaning.

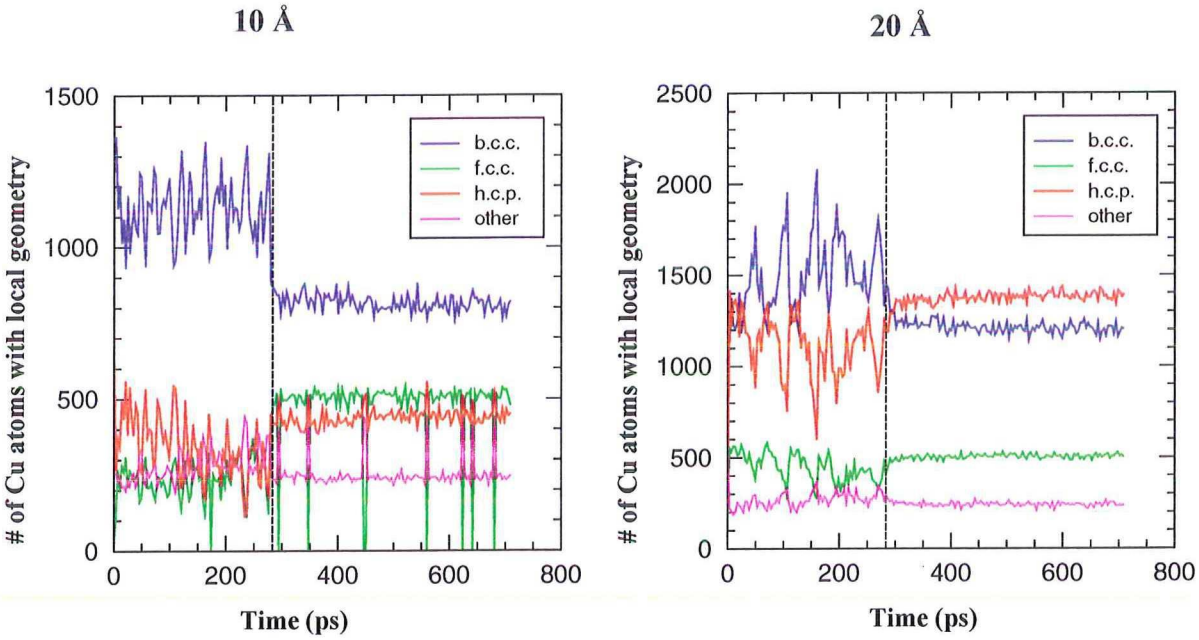

Fig. 26. Number of Cu atoms with a certain local geometry: b.c.c./f.c.c./h.c.p. or unidentified for several configurations of the 10 Å and 20 Å layers at 300 K in the simulation period. Dashed line indicates the moment of the last 75 eV He impact.

unidentified. This agrees reasonably with the geometry after the start of the simulation. The first data point (at 0 ps) is irrelevant. The local geometry at 300 K during 75 eV He bombardment in the 20 Å Cu layer is given as reference in which the structure does not change visibly during bombardment. Here it is interesting to note that in the entire course of the bombardment at 300 K more Cu atoms have been displaced (over the usual large distance: 1.88 Å) in the 10 Å Cu layer than in the 20 Å Cu layer (respectively ~1000 against ~400 atoms). This is an indication that is at least possible that the microstructure of the layer slightly changes. However, the shapes of the mean potential energy against time of the 10 Å and 20 Å Cu/Mo films do not differ when shifted so that the data overlap.

At 1200 K even more helium atoms trap in the molybdenum substrate: a total of 7 He atoms are substitutionally trapped in the 4th (1 He), 5th (3 He) and last Mo plane (3 He). One of these He atoms shows similar behaviour to a phenomenon earlier encountered by Klaver [7]. This He atom is not directly trapped substitutionally, but moves interstitially in the Mo for 28 ps before a RCS of a few Mo atoms is started towards the interface and the He atom becomes trapped substitutionally. The kinetic energy of the He atom, when it is injected in the film, does not drive this mechanism for after 28 ps the kinetic energy of the impact is long lost by collisions. The other six He atoms become much faster substitutionally trapped (<3 ps). In Klaver a similar effect of 100 eV He atoms on a Mo (100) film (both evaporated and deposited with argon assistance) is described: an interstitial situated He atom can draw a vacancy from the surface or attract a vacancy to the He atom which is subsequently substitutionally trapped. The surface or vacancy has to be in close range of the interstitial He atom (less than 3 Mo atoms). This mechanism is attributed to the stress caused by the interstitial He atom. In our case the interface evidently acts the same way as the surface.
The 10 Å Cu layer also randomizes by the 75 eV He bombardment at 1200 K (except at least the 1st and 2nd plane) and when the bombardment is completed recrystallization sets in. The activation energy of this last process is 0.68 eV (see previous section for the calculation

method). Only two He atoms are still trapped in the Cu layer at the end of the simulation, see Fig. 25. They are trapped in a defect of over 7 substitutional sites (see for depth Fig. 25). Just after the bombardment 9 He atoms were trapped in the Cu layer in the 2nd and 3rd plane: in a monovacancy, a divacancy, 2 trivacancies and 2 defects (of over 5 and 9 sub. sites) respectively filled with 1, 1, 1, 2 and 3 He atoms. Striking is that at both moments no He atoms are trapped in the first Cu plane. The 7 He atoms that leave the film during the relaxation phase of the run depart in the same way as in the 20 Å Cu layer: sometimes in groups at about the same moment. Five He atoms leave in 1.6 ps via vacancy diffusion: a path to the surface exists for a short time. Also interesting is the motion of Mo atoms that are relocated in the first Cu layer due to the He atoms: two of these Mo atoms move quite a distance (7 and 11 Å) during the relaxation phase.
Comparing the bombardment of the 10 Å and 20 Å Cu/Mo films the following conclusions are drawn: in the 10 Å Cu/Mo film He atoms reach the Mo substrate in contrast to the 20 Å layer where in no case He atoms are found in the Mo substrate. Only few He atoms (2) remain trapped in the 10 Å Cu lattice at 1200 K. In the 1200 K, 20 Å run more atoms remain in the Cu layer: 8 He atoms (also in the ideal and IBAD 20 Å Cu layers). This is probably the influence of the near surface.

Relation between thickness and influence of temperature and bombardment
The reaction of the lattice on temperature and/or extra energy transfer due to the He atoms is dependent on the thickness of the deposited Cu layer. This can be concluded from the following observations.

- At 1300 K the 20 Å EVAP copper layer randomizes without He bombardment (Sec. 3.3.1). At this same temperature the 47 Å IBAD Cu layer stays intact. Whether the layer is deposited with or without argon assistance is not decisive in this comparison, because both the 20 Å EVAP and IBAD Cu layers randomize temporarily by a 75 eV He beam at 1200 K and thus react the same to this temperature and He bombardment. The 47 Å Cu layer (IBAD) does not randomize completely even with 75 eV He bombardment (24 He atoms have impacted). Only the first 9 Cu planes disorder of a total of 25 Cu planes.
- The 75 eV He bombardment in the 10 Å Cu layer at 300 K has displaced more atoms (over the usual large distance: 1.88 Å) than in the 20 Å Cu layer (respectively ~1000 against ~400 atoms).

In Table 8 the reactions of the various Cu lattices of the runs in Table 4 to the He bombardment are given for an overview. The thickness of the deposited Cu layer is relevant to the reaction to the temperature and He bombardment. This conclusion is supported by Fig. 27 in which the potential energy per plane is given for the 10 Å, 20 Å and 40 Å Cu/Mo films and the 34 Å ideal Cu film. The dotted line represents the last Mo plane if a substrate is present, the numbering continues for the Cu planes. The mean potential energy per plane $\langle U \rangle_p$ is much lower for the Mo substrate and is not depicted. The first Cu plane (plane 7) is tightly bound to the underlying Mo substrate. The increase in $\langle U \rangle_p$ at the highest Cu planes is of course the influence of the surface. The mean potential energy in the second Cu plane (plane 8) of the Cu/Mo films is less negative in comparison to the remaining Cu planes (except the surface planes). The influence of the interface can be clearly seen in the 40 Å Cu/Mo film without He bombardment: $\langle U \rangle_p$ slowly decreases over 6 planes to the lowest value (plane 14) which is very near the value of the ideal Cu film. The surface stretches over

Table 8. Overview of the reaction of the Cu lattice for several layer thicknesses at temperature and bombardment. Bombardment and relaxation take place at the same temperature. Exact description of the runs can be found in Table 4.

He bombardment	***10 Å***	***20 Å***	***40 Å***	***47 Å***
300 K	microstructural change	no change		
1200 K	randomization and recrystallization	randomization and recrystallization	no change yet (limited fluence, 1000 eV)	
1300 K		randomization without He bombardment		first 9 planes randomize (limited fluence)

five planes according to $\langle U \rangle_p$ in this 40 Å layer. This explains the high values of $\langle U \rangle_p$ for the 10 Å and 20 Å Cu layers: the total number of planes in these layer is small and still within the influence of both the interface and surface. Although the relation between the binding energy and the energy that is needed for a transition (such as the jumping of an atom to another site) is not always correlated linearly, the binding energy supports the earlier conclusions of the dependence of the thickness of the deposited Cu layers of the Cu/Mo films.

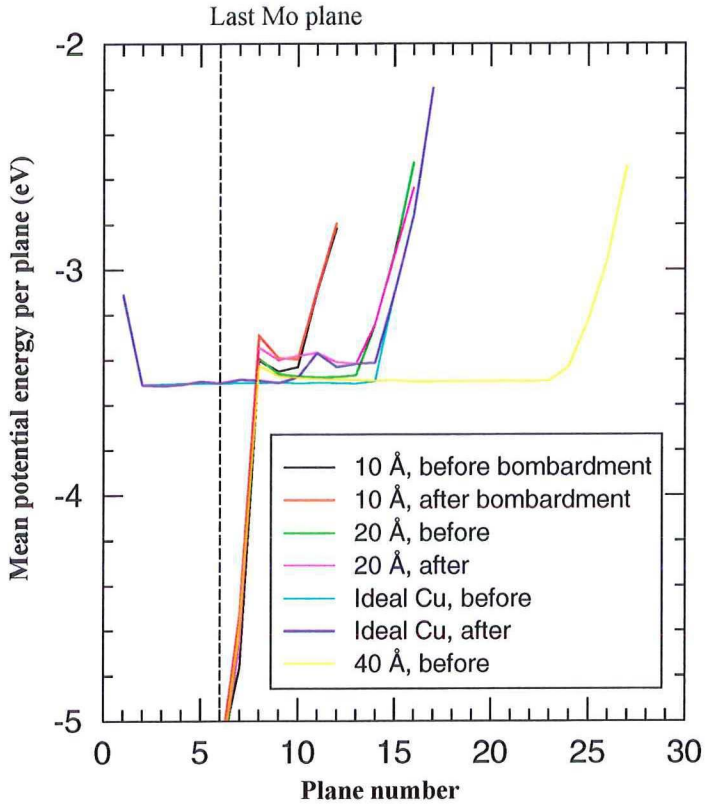

Fig. 27. Mean potential energy per plane for several runs with various layer thicknesses. The numbering continues for the Cu planes instead of the usual renumbering. All data proceeds from configurations at 300 K.

4.3.2 Growth method

Dislocations have been found in both EVAP and IBAD 20 Å Cu/Mo films. The repetition of certain defects in the planes shows the location of edge dislocations in the 20 Å EVAP Cu layer, see Fig. 28 B in which such a defect is shown in the 4th plane. The extra rows of Cu atoms that are part of the edge dislocation are illustrated with aid of the lines. In Fig. 28 A all extra rows of Cu atoms are enlarged depicted, the arrows indicate the 'core' of the

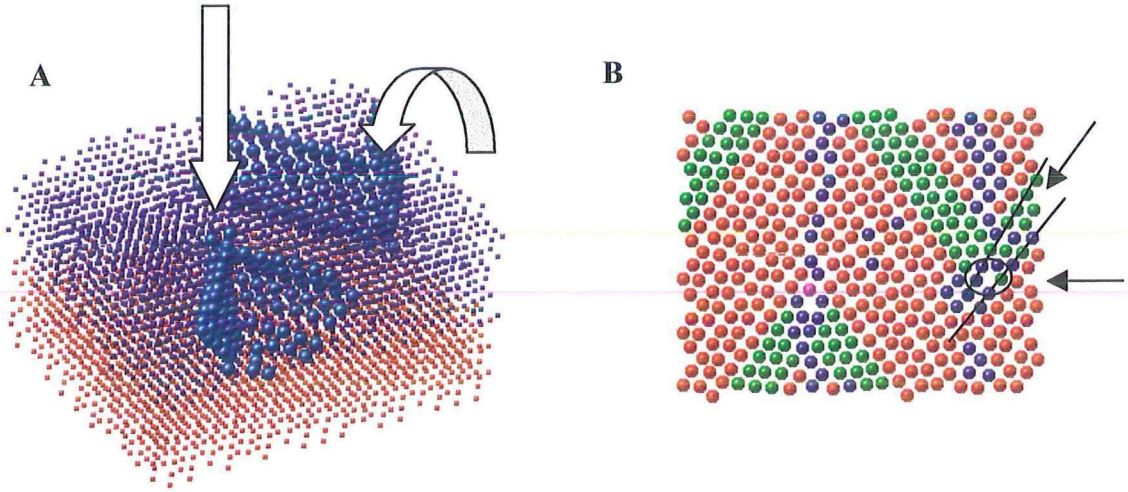

Fig. 28. A. Edge dislocations in the 20 Å EVAP Cu layer (blue) on Mo substrate (red) at 300 K before bombardment. Rows of extra Cu atoms are enlarged depicted; arrows show 'core' of dislocations. B. Space at the end of the row extra Cu atoms is illustrated with aid of arrows and lines. Colouring according to local crystallographic geometry: green = f.c.c., red = h.c.p., blue = b.c.c. and pink = unidentified.

dislocations. The dislocations in the 20 Å ion assisted Cu layer are somewhat different, for they have a partial screw and edge character. This is illustrated in Fig. 29. Colors indicate separate planes. The four top planes are not depicted of this thin film. The right figure is a magnification of the right figure. Not only an extra row of Cu atoms is observed in-plane which indicates an edge dislocation, but also two Cu rows verge downwards and connect with the previous plane. This indicates a screw dislocation. The dislocation shown in the figure is thus of mixed character. The white arrows represent the Burger's vector of the edge (horizontal arrow) and screw character of this dislocation. In larger Cu/Mo systems (see Sec. 3.1) both EVAP and IBAD 20 Å Cu layers have dislocations with partial edge and screw character. In the 10 Å EVAP Cu layer dislocations have not yet evolved; extra rows of Cu

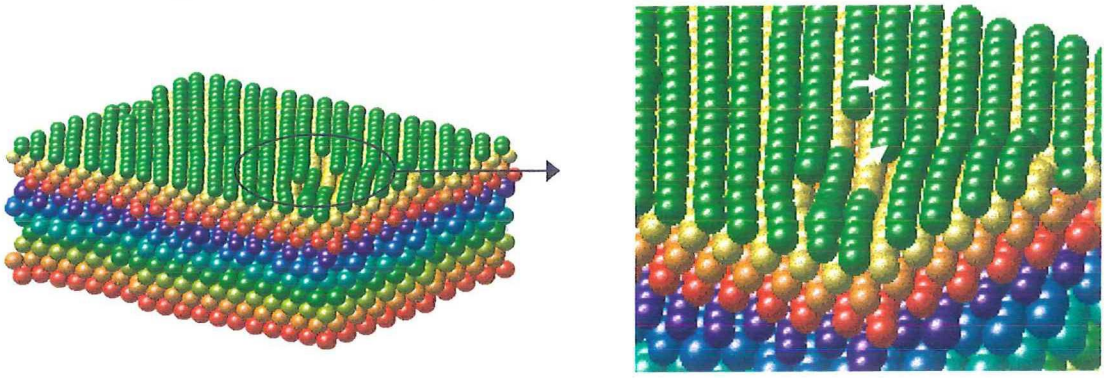

Fig. 29. Section of 20 Å IBAD Cu layer showing dislocation with partial edge and screw character. Four top planes are not depicted. Colors indicate separate planes. White arrows are the Burger's vector of edge (horizontal) and screw (vertical) character of dislocation. Mo atoms are enlarged depicted. The configuration is cooled.

atoms can be found occasionally in the planes, but repetition of this structure through the planes has not been observed.

As mentioned before the 20 Å IBAD Cu layer randomizes also by bombardment at 1200 K (except the lowest three Cu planes). Just after the bombardment at 1200 K 17 He atoms have trapped in the 20 Å ion assisted deposited Cu layer by creation of defects (7 He more than in the EVAP layer). Four He atoms are trapped in monovacancies (single filled), 3 He in divacancies (single filled), 1 He in trivacancy and 7 He in 3 defects of more than 7 substitutional sites. These defects are spread over the first 5 Cu planes. Two He atoms reside in monovacancy connected to an extra row of Cu atoms. Recrystallization sets in after bombardment: the activation energy measured by the decrease in mean potential energy is 0.75 eV and five He atoms leave the film in two groups after the bombardment. At the end of the run only 2 monovacancies (single filled), 1 trivacancy (1 He), two defects of ~6 substitutional sites (with 2 and 3 He) and a large defect with 4 He (over 9 sub. sites) remain. These defects are found in the 1st-3rd Cu planes. The centre of distribution does not change. Though the interface is mixed in the IBAD layer (see Sec. 3.1), in both EVAP and IBAD 20 Å Cu layers the centre of the distribution of the trapped He atoms is in the second Cu plane after the complete run. Concluding the comparison with the 20 Å EVAP Cu layer: even more He atoms are found trapped in the 20 Å IBAD layer and there is no apparent difference in the influence of the interface on the trapped He atoms.

4.3.3 Ideal copper thin film

Here we will treat shortly the ideal copper (111) thin film bombarded at 300 K with 75 eV He atoms. The encouraging results of the 20 Å layer of relaxation at 1200 K induced to simulate the relaxation of this run also at 1200 K. However, extensive analysis of this simulation has not been performed yet. Nevertheless, the behaviour of the He atoms in the relaxation phase is very interesting for comparison with the TDS experiments and we would not refrain these first results. This f.c.c. Cu film consists of 15 planes (33 Å); this is about the size of the 20 Å Cu + 14 Å Mo thin film and the film has no inherent defects. The surface is free; in lateral directions there are periodic boundaries. Simulation of the (111) orientation was chosen since the deposited Cu layers resemble most with this orientation.

At the end of the bombardment at 300 K 17 monovacancies (all except 3 vacancies

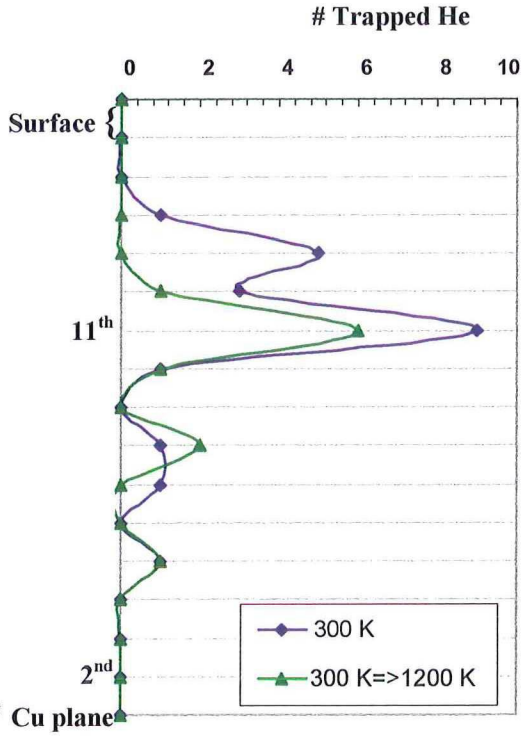

Fig. 30. Number of He atoms per plane in the 33 Å ideal Cu film at 300 K and after relaxation at 1200 K. The connecting lines between the datapoints are given to discern both temperatures, but irrelevant qua physical meaning

filled with 1 He atom), 4 divacancies (3 single filled and 1 double filled) and 2 trivacancies (single and double filled) are present. All 22 He atoms are substitutionally trapped. See Fig. 30 for the distribution of the trapped He over the planes at 300 K and at the end of the relaxation at 1200 K (relaxation period is 355 ps). Three He atoms trap at a considerable depth: > 17 Å. Interestingly, at this depth the first interstitial situated He atom is found, this atom resides 149 ps at an interstitial site before a substitutional site is created by a short RCS of Cu atoms. In this mechanism the existence of a spike does not play a role for the kinetic energy is long lost after this time, stress is more likely the driving force of this mechanism. The bombardment roughens the Cu film. During the relaxation at 1200 K 11 He atoms leave the lattice thermally. Again the same mechanism as in the 20 Å deposited Cu layer is observed: departure/motion of He atoms via vacancy diffusion. The remaining He atoms trap in 6 monovacancies (single filled), 2 divacancies (single filled) and 3 He atoms in 1 large defect (over 10 substitutional sites in the 11^{th} and 12^{th} plane). In both '300 K => 1200 K' In Fig. 4.3.7 can be seen that the He atoms leave the upper planes. The center of the distribution (largest number of He atoms per plane) does not alter in contrary to the behaviour of the He in the relaxation at high temperature of the 20 Å EVAP Cu layer where the He atoms 'gather' in the 2^{nd} Cu plane. Another difference with both the 10 Å and 20 Å runs is that a few He atoms in this ideal film (without Mo substrate) trap deeper (for all temperatures).

Table 7. General data of He bombardment. All values are calculated at the end of the bombardment, except the percentage of thermal leavings.

	300 K, 10 Å	***1200 K, 10 Å***	***1200 K, 20 Å, IBAD***	***300 K, ideal Cu***	***300 => 1200 K, ideal Cu***
% He left behind in film	23 %	16 %	17 %	22 %	22 %
% Thermal leavings	0 %	7 %	5 %	0 %	11 %
Backscattering	76 %	84 %	83 %	78 %	78 %
Transmission	1 %	0 %	0 %	0 %	0 %
Cu sputtering yield	0.23	0.15	0.21	0.21	0.21

5 Simulation and TDS experiment

In the first section the main results from the Thermal Desorption Spectrometry experiments will be introduced, followed by ideas/results from the simulations (see previous chapter) to help interpret these experimental results. The degree of agreement in the simulations and experiment for the various phenomena will be indicated. In the second section an overview of all important limitations for results is given.

5.1 Simulation and TDS experiment

Main experimental results

Fig. 31 shows the thermal desorption spectra in which the copper layer thickness is varied for decoration energies of 75 eV and 1000 eV. The experimental spectra for which simulations of helium bombardments with the same film thickness and implantation energy were performed

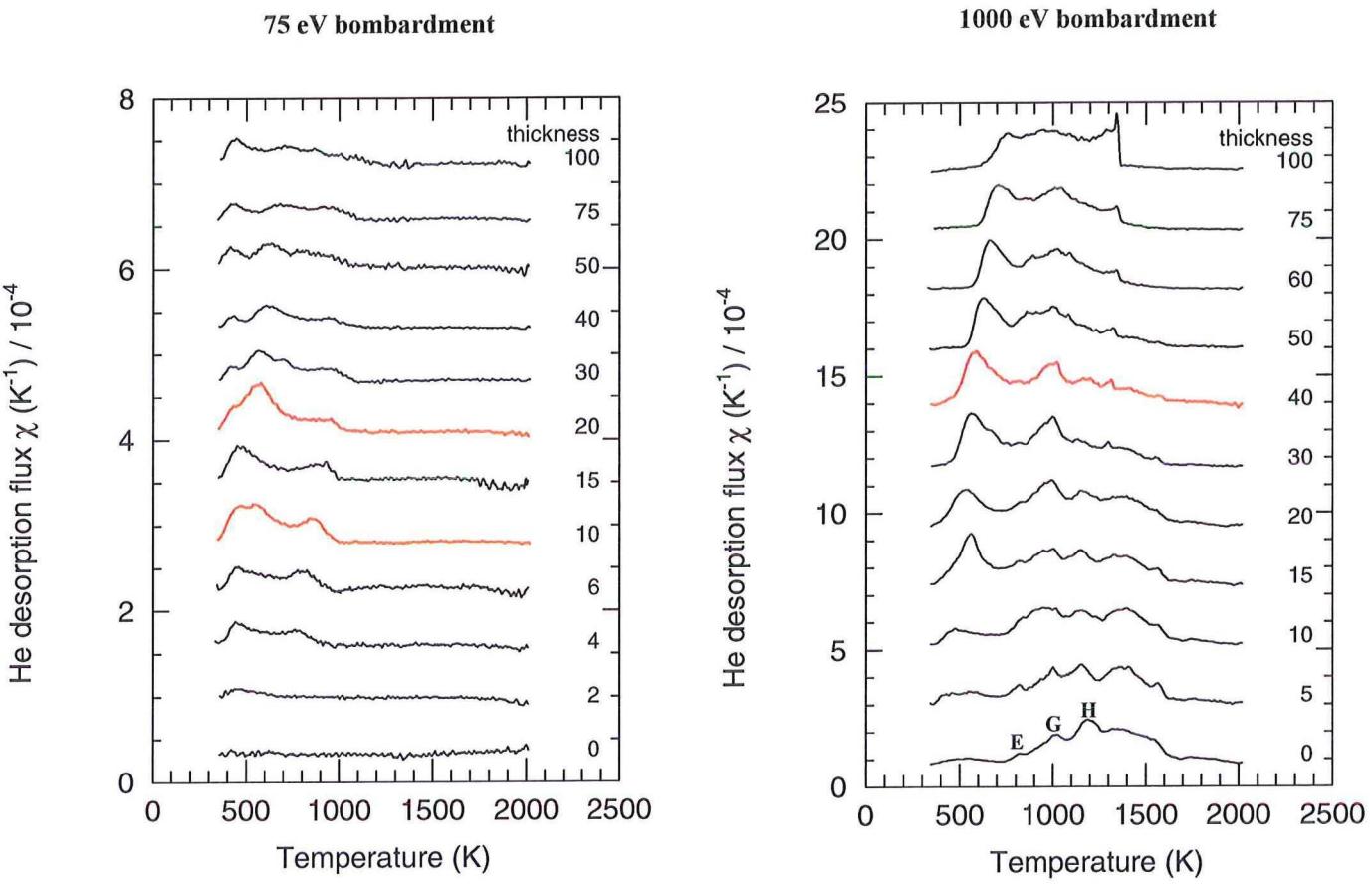

Fig. 31. Normalised helium desorption spectra for various film thicknesses decorated with helium atoms with an energy of 75 eV and 1000 eV. The fluence is 2.10^{14} He/cm^2 (without secondary electrons correction) and the heating rate is 40 K/s. Simulations of He bombardment have taken place at the same film thickness and energy for the spectra colored red. The thickness is given in Ångstroms. See text for explanation of letters E, G and H.

are colored red. It is important to bear in mind that the actual desorption has not yet taken place in the simulations (see last part of Sec. 2.1). Roughly, the outcome of the simulations (after relaxation) can be compared with the start of the experimental spectra. An annealed molybdenum substrate is bombarded when no copper is deposited. The spectrum of polycrystalline molybdenum (orientation is mainly (110)) bombarded by 1000 eV He atoms is elucidated by among others van der Kuur [19]. The peaks at about 800K (E), 1000 K (G) and 1200 K (H) are all appearances of the monovacancy, respectively multiple, double and single filled with He atoms. The ridge after 1300 K is associated with vacancy clusters. The cluster size and filling are not precisely known. Striking in the 1000 eV spectra is the shape of the peak at 1350 K for layers thicker than 30 Å; it is much sharper than all other peaks. This peak becomes more pronounced for thicker copper layers. For thicker Cu layers (> 200 Å, not shown) this peak further increases. The melting/sublimation temperature of Cu lies at 1358 K. Buters [20] performed TDS experiments on a single copper(100) crystal and concluded that helium desorbs from single filled monovacancies at 780 K, multiple filled monovacancies at 610 K, and a desorption peak at 700 K is attributed to the desorption of helium from double filled divacancies.

Creation of defects by 75 eV He beam ⇔ Inherent defects

In Sec. 4.1 we have concluded that 75 eV He bombardment displaces copper atoms and creates defects, which is contrary to the starting point of the TDS experiments. This is most unambiguously seen in the simulations of ideal f.c.c. copper at 300 K; here the influence of the temperature in the simulation and inherent defects/disorder/growth of the lattice are ruled out as possibly enhancing factors of this phenomenon. Stress is probably the driving force of this mechanism. At the end of Sec. 4.3 the bombardment at 300 K and subsequent relaxation at 1200 K of this ideal f.c.c. film is specified. Half of the He atoms that create defects in the bombardment in the film desorb during the relaxation from the upper planes of the film. The mechanism of this desorption is vacancy diffusion. At the end of the relaxation He atoms still remain in vacancies that were not present before implantation; the total trapped He fraction is 11%. This implies that in the TDS experiments for films that have been grown at high temperature or that have been heated so that no inherent defects are present, the 75 eV ion beam should also create defects and that the spectra should at least show some peaks. In this the experimental results are still being debated. In Buters [20] spectra of an perfect copper(100) single crystal and of an annealed crystal after deformation strongly resemble each other and have a series of peaks from 350 K to 650 K by 75 eV He bombardment. The spectrum denoted with a C in Fig. 32 shows this spectrum, the

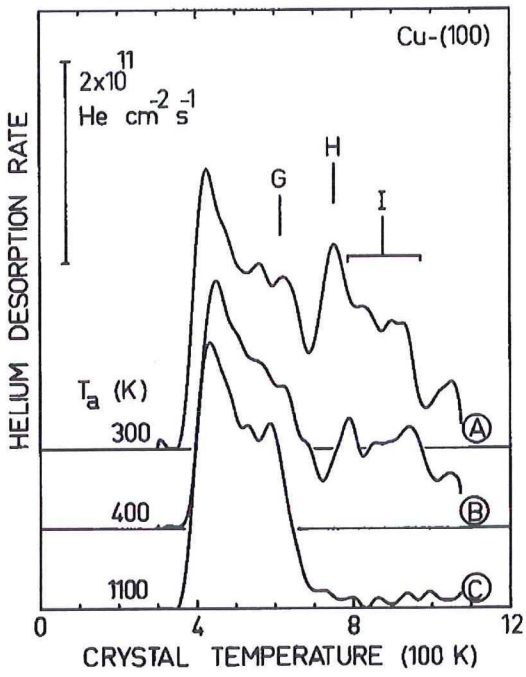

Fig.32. Spectrum © is the desorption of 75 eV He bombardment of annealed copper single crystal (almost identical to a perfect Cu single crystal). Measured by Buters [15].

fluence in this experiment is 4.10^{14} He/cm^2 and the heating rate of the temperature ramp is 40 K/s. The total trapped fraction of spectrum C is ~0.4% (calculated by integrating the area of the peaks normalized in heating rate and fluence). Notice the difference of orientation in our simulated film (111) and the Cu(100) crystal in the experiments of Buters. In our present measurements no peaks are present in the spectrum of a 200 Å Cu layer on Mo substrate deposited at 800 K (not shown). One expects no inherent defects are present in this Cu layer due to this high deposition temperature. These experimental results for copper do not agree with the TDS results of Buters which are currently not understood, unless a (100) crystal surface behaves differently from a Cu layer grown on a Mo substrate. The simulation results resemble most with the experimental results from Buters (since both have peaks in the (predicted) desorption spectra). However, the total trapped fractions in the simulation is much larger than in the experiment of Buters. This difference can indicate either that the mechanism of the creation of defects by 75 eV He beam is exaggerated in the simulations or that the relaxation at 1200 K does not present enough opportunities for diffusion etc. (in connection to the He desorption) for comparison with 300 K experimental results. The results of the experiments in ideal films are inconclusive, therefore it cannot be confirmed nor rejected that a 75 eV He beam creates defects.

Vacancy diffusion ⇔ Interstitial desorption

Two observations indicate another desorption mechanism than the usual dissociative mechanism of the TDS experiments (desorption by dissociation from a trap by a He atom and a subsequent escape from the lattice by interstitial movement) is also important.

- In the simulations only one observation of a temporary interstitial situated He atom has been made in the Cu layers (deep in ideal Cu film, see Sec. 4.3.3), in all other observations He atoms resided at substitutional sites. In the Mo substrate relatively more observations of interstitial He atoms were made.
- During the relaxation at 1200 K in both the 20 Å layer and the ideal Cu film (see respectively Sec. 4.2 and 4.3) after bombardment at 300 K about half of the trapped He atoms escape the lattice due to vacancy diffusion.

The simulations indicate that desorption of He atoms due to vacancy diffusion in copper layers is dominant at a low temperature (bombardment in the experiment at 300 K is simulated) compared with the dissociation mechanism in which the He atoms thermally escape a trap and interstitially leave the lattice. A remark has to be made: the actual desorption mechanisms at high temperatures in the experiment are not known. The mechanisms can be quite complex: He movement via vacancy diffusion (both desorption and interaction with other vacancies and He atoms which can change the desorption energies), thermal escapes from various vacancies with several desorption energies, retrapping, creation of vacancies when the vacancy formation energy is feasible. Not only the presence of vacancies is important for the effect of vacancy diffusion, but also the rate of diffusion. During the temperature ramp the vacancy diffusion increases.

The sharp peak in the 1000 eV TDS measurements can be interpreted with the aid of this mechanism and the following observation from the simulations which is an effect of the vacancy diffusion: during the relaxation at 1200 K after bombardment at 300 K of both the ideal Cu film (Sec. 4.3) and the 20 Å EVAP Cu layer (Sec. 4.2) a tendency to cluster is noticed. Just after the bombardment in both films defects of a maximum size of four substitutional sites are present. After the relaxation in the ideal Cu film a defect of over 10

sub. sites (with 3 He atoms) is found and in the 20 Å deposited Cu layer a defect of over 5 sub. sites (filled with 2 He). This tendency is also present in the runs with the 20 Å Cu layer completely at 1200 K and 1300 K; here the layer is (temporarily) randomized. This seems to amplify this tendency (see Sec. 4.2). In the 1200 K 10 Å run this tendency is not directly observed in comparing the size of the defects in the configurations just after bombardment and when the run is completed.

Returning to the sharp peak in the 1000 eV spectrum, the following explanation is supported by the tendency to cluster via vacancy diffusion. The shape of the peak is quite different from all the other peaks and suggests an immediate and simultaneous desorption of all He atoms that are still present (zero order desorption). The desorption temperature of this peak is ~1350 K which is very close to the melting point of copper. At the pressure in the experiment ($\sim 1.10^{-10}$ mbar) the Cu lattice probably vaporizes and all He atoms that are still trapped are released. The clustering via vacancy diffusion prevents the He atoms from an earlier desorption because desorption from a vacancy cluster requires much more energy than from mono and divacancies [24]. For the formation of these large defects a large number of vacancies in the Cu layer is required and a certain thickness of the Cu layer (otherwise the He 'bubbles' can not form because the small defects escape earlier due to nearness of the surface). The peak at 1350 K increases with the thickness of the deposited Cu layer, this is according to the theory of the clustering via vacancy diffusion, because more vacancies are created in the Cu layer and fewer in the Mo substrate as the thickness increases. The peak also increases with an increasing fluence (spectra in which the fluence is varied are not shown) and this is also according to the mechanism of increased clustering by more vacancies and He atoms in the Cu layer. In the 75 eV spectrum this is not seen, since the number of (created) defects is much smaller and less deep in the layer. Buters has not measured the sharp peak, for the temperature at the end of the heating was taken only 1100 K.

In connection to the vacancy diffusion one other remark can be made: if the rate of the vacancy diffusion in the relaxation runs at 1200 K seen in the simulations is even approximately correct, vacancies in the first atomic plane from the surface as seen in the TDS experiments on molybdenum by van der Kuur [19] will not occur in the copper layers. In the runs at 1200 K the He atoms are trapped from the 6^{th} plane from the surface and further (the 1200 K 10 Å is an exception in this; here helium are trapped from the 4^{th} plane). Here uncompleted planes are also accounted for in the plane numbering. Another possibility is that the vacancy diffusion is somewhat overrated in the simulations and part of desorption of the first peak in the 75 eV spectra is actually observed. Overlayer experiments can give answers about desorption mechanisms and depth, but as earlier concluded by Buters [20] detailed studies are hindered by the narrow temperature range of the spectrum.

Another escape route: dislocations?

In van der Kuur [19] a fast escape mechanism for He atoms is proposed: columns with grain boundaries act as diffusion paths for He atoms. The total fraction of He atoms that trap reduces by these fast escape routes. In Fig. 31. a similar reduction can be seen for thicker Cu/Mo films in the 75 eV bombardment. Fig. 33 shows all available measurements for the 20-50 Å Cu layers decorated with 75 eV He impacts. Here again this reduction in the total trapped fraction is shown. The turning point is around the thickness of 30 Å. In the simulations dislocations are identified in both the 20 Å evaporated and ion assisted deposited Cu layers. In thinner Cu/Mo films the microstructure is not yet fully developed; for example

the dislocations are not yet present as in the 20 Å films (see Sec. 4.3.2). It has been established the microstructure is fully developed around 20-25 Å. This layer thickness is near the value in the experiments for which the total trapped fraction decreases. The dislocations acting as fast diffusion paths are a reasonable explanation for the found reduction. No decrease has been found in the total trapped fractions of the 10 Å and 20 Å runs of the simulations. Extensive analysis of the exact route of escape (for instance via a dislocation) has not taken place yet for the 300 => 1200 K, 20 Å run.

Bombardment of Cu/Mo films

In this section the simulation runs will be compared more closely to the experimental results. The total trapped fraction in the 75 eV bombardment of the 10 Å EVAP Cu layer in the simulation is 9% (the complete run is performed at 1200 K), in the experiment 2%. The total trapped fraction in the simulation of the decoration of the 20 Å Cu layer is 8% (bombardment at 300 K, relaxation at 1200 K), in the experiment also about 2%. These trapping fractions agree much better with the experiments than the fractions in the ideal Cu crystal (simulation: 11 % and in experiment of Buters: 0.4%). The range of the total trapped fraction for the 1000 eV run is 14-58%, respectively depending on the escape or trapping of the interstitial He atoms in the Mo substrate and the He atoms that have passed through the thin film. The total trapped fraction in the experiment ranges from 11-31%. The first value is corrected for the slightly changing sensitivity of the mass spectrometer. The last value is measured. Note that the fluence of the 1000 eV run is still limited (1.10^{13} He/cm^2); the fluence in the 1000 eV spectrum is 2.10^{14} He/cm^2 . At this low fluence it is likely the spectrum shows hardly any peaks (supported by a measurement at this fluence in 200 Å Cu layer, not shown).

The centre of the distribution of the defects after bombardment at 300 K and subsequent relaxation at 1200 K in the ideal Cu crystal surface and the 20 Å Cu/Mo film differ: the second Cu plane near the Cu/Mo interface 'attracts' defects (see Sec. 4.2). In the ideal crystal such a phenomenon has not been observed. If one assumes the spectrum of the ideal Cu film of the simulations resembles the spectrum measured by Buters [20], see Fig. 32 spectrum C (that is a series of peaks from 350 K to 700 K), the main difference between the experimental 20 Å, 75 eV spectrum (Fig. 31) and

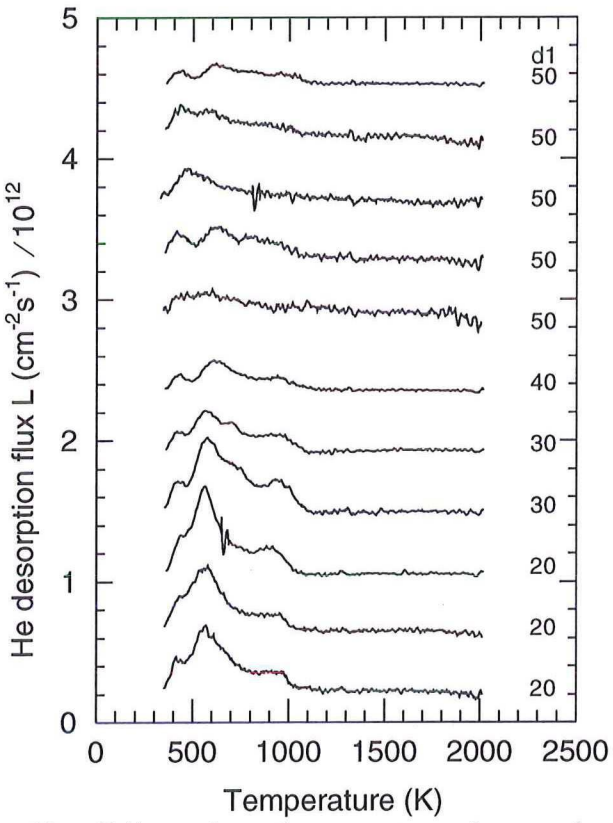

Fig. 33. Helium desorption spectra of several measurements of film thicknesses of 20, 30, 40 and 50 Å (d1). The film are decorated with helium atoms with an energy of 75 eV, the fluence is 2.10^{14} He/cm^2 and the heating ramp is 40 K/s.

the spectrum of Buters is the peak at ~950 K in the 20 Å, 75 eV spectrum. It is likely that this peak is connected with desorption of He atoms from defects near the interface of the Cu/Mo film. The shift of this peak to higher temperatures for increasing thickness has been explained extensively in [16]. Resuming, an increased distance to the surface, an increased diffusion length that amounts to larger defects and change in film stress and structure are of influence on the shift of the peak. In the 20 Å, 1000 eV spectrum this 'interface' peak is less recognizable since at this temperature also peaks originating from desorption from the Mo substrate are present.

For molybdenum there is also no experimental agreement in the presence of peaks at subthreshold He bombardment. Van der Kuur [19] has recorded a broad peak at 420 K in an annealed polycrystalline molybdenum substrate by 100 eV He subthreshold bombardment (fluence is 1.10^{14} He/cm^2). It has been determined that this peak is indeed created by the ion beam and it represents monovacancies in the first 5 Å from the surface. In the present measurements, see Fig. 31 with no grown copper layer (0 Å), no peaks are observed for an annealed polycrystalline molybdenum substrate.
The overlayer experiments of van der Kuur [19] show that by depositing an 5 Å Mo layer over an already bombarded thin Mo film the surface peak for the most part reappears as G and H peaks from desorption of monovacancies. We expect that the deposited Cu layer acts the same way as a Mo overlayer and therefore, we would see G and H peaks of the desorption from Mo in for example the 10 Å Cu/Mo spectrum. This is not the case (Fig. 31) and it is in contrast to the simulation results of the 10 Å Cu/Mo film in which for both runs at low and high temperature He atoms trap in the Mo substrate. A possibility in which the simulations agree more with the experiments, is that the He desorb at a low temperature from the Mo substrate and get trapped in the second plane of the copper. Another explanation is that the He atoms do not trap in the Mo substrate in the 10 Å Cu/Mo film just as in the annealed substrate (0 Å) (contradictory to the simulation results).

In all runs no defects were found in which the number of He atoms exceeds the number of substitutional sites in the defect. This is contrary to the TDS experiments where for example multiple filling of a monovacancy is described [24].

5.2 Discussion

In Fig. 34 a critical overview of all possibly relevant limitations of the simulations and the experiments is given. Striking in the results is that the helium atoms often do not act as predicted. Combining a few observations leads to the following arguments for questioning the used He-He, He-Cu and He-Mo potentials:

- No observations are present in which the number of He atoms in a defect is larger than the number of substitutional sites of the defect for both Cu and Mo (also in Klaver [7]).
- So far only one (temporary) interstitial situated He atom is observed in the Cu lattices.
- The creation of defects by 75 eV He irradiation in the extent seen in the simulations is not supported by the TDS experiments.

Though not all these observations lead directly to a doubtful He-He interaction, together with a recent comparison of several He-He interaction potentials in [25] in which our He-He

interaction turned out to be more positive than the other potentials in the range of 1-3 Å (and thus more repulsive), there is enough reason to recommend an additional investigation of this potential. From the Fig. 34 and the remaining questions in the previous chapter it becomes clear that the short simulation times are still a serious limitation.

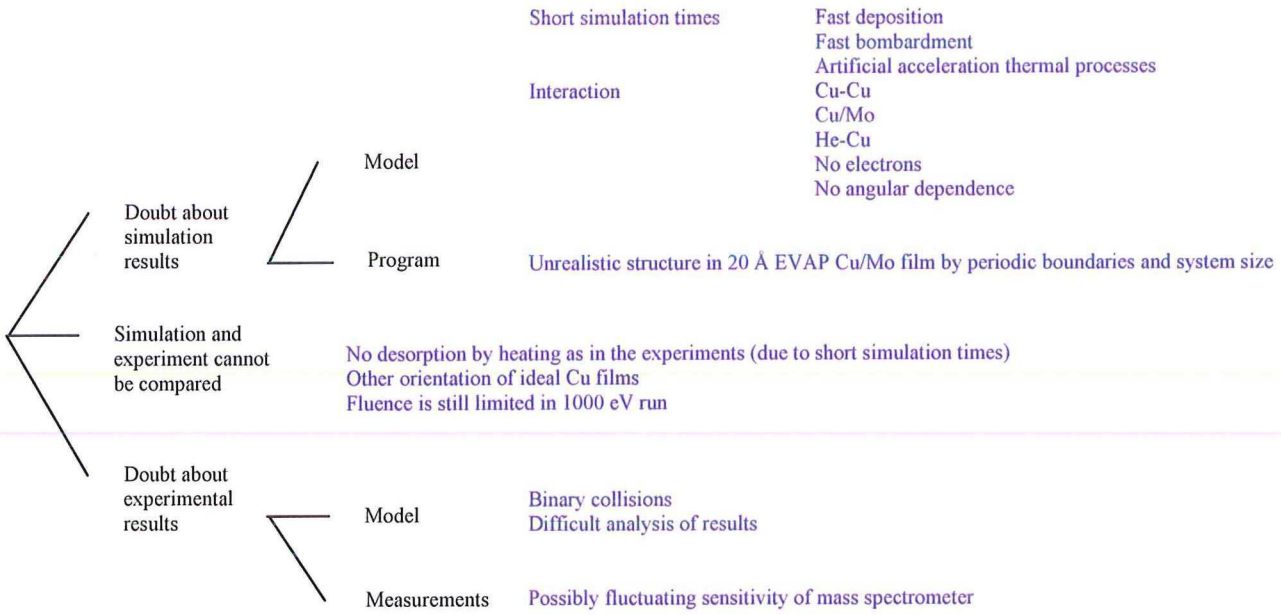

Fig. 34. General overview of possibly relevant limitations in this research.
-- = Rough classification
-- = Limitations

6 Conclusions and recommendations

6.1 Conclusions

Simulations of low energy He bombardment and subsequent relaxation were performed to probe defects of Cu and Cu/Mo films as in the experimental technique of thermal helium desorption spectrometry.

Molecular dynamics simulations show directly several processes at atomic level such as helium impacts. This has been a very instructive element in this research. In the simulations copper has turned out to be more reactive than for example molybdenum, which has been part of the group's research programme before the copper investigations. Thin Cu/Mo films (in this case 10 Å and 20 Å Cu deposited on a Mo substrate) for example, randomize by fast 75 eV He bombardment at 1200 K in the simulations. One of the major limitations of the molecular dynamics simulations is still the limited simulation time, in our case ~1 ns. To reduce this limitation, most simulations have been performed at a high temperature (1200 K) to activate the same processes that occur in the experiments at 300 K. The above mentioned randomization at 1200 K is viewed to be unrealistic; He bombardment at 300 K and subsequent relaxation of the films at 1200 K seems a better alternative.
Not only the randomization has been surprising, also the creation of defects by the 75 eV He beam in both the Cu/Mo films and the ideal Cu crystal was unexpected in view of the binary collision theory that is frequently used in TDS experiments. The subthreshold bombardment is intended to reveal the inherent defects of the films. In the simulations in both copper and molybdenum displacement by subthreshold helium irradiation has been found [7], only in copper to such extent that it becomes urgent to establish whether the modeling in the simulations is correct in this respect. In the examined ideal Cu surface layer and the Cu/Mo films subthreshold He bombardments displace Cu atoms via replacement collision sequences and trap in the space of the emerged Frenkel pair. Point defects are created. Not only close to the surface, but also in the 'bulk' of the ideal Cu film trapped He atoms are found. During relaxation at a 1200 K about half of the He atoms that were trapped escape via vacancy diffusion. Other simulations [23] support the displacement of Cu atoms by low recoil energies. The presence of He atoms in defects in the simulations implies that in a spectrum of these results at least a peak(s) is present. The spectra of the TDS experiments are inconclusive in the existence of the by the simulations required peak(s). Moreover, if the simulations are compared to the measurements [20] that most resemble the simulations for the ideal Cu film (in which this creation of defects is most evident for no inherent defects were present), the total trapped fraction of He atoms does not agree with the experiment, respectively 11% and 0.4%. This disagreement can originate both from the bombardment and from the relaxation phase of the simulations, respectively because of a too positive modeled interaction with He atoms and because of an incorrect rate of process acceleration. A less likely cause is the difference in surface orientation between the experiment and simulation. The total trapped fractions in the Cu/Mo films agree much better with the experiments, respectively 9% and 2% for the 10 Å Cu layer and 8% and 2% for the 20 Å Cu layer.

Several ideas were generated from the simulations to assist the interpretation of the TDS spectra of the Cu/Mo films. One of the most prominent peaks (at ~1350 K) in the 1000 eV spectrum in which the thickness of the deposited Cu layer is varied, can be explained by the

clustering of defects via vacancy diffusion in copper in the relaxation at 1200 K with such a high stability that they remain present up to the sublimation point and the relative deep impacts of 1000 eV He atoms. The concentration of defects in the second deposited Cu plane can explain the last peaks in the 75 eV spectra of the 10 Å and 20 Å Cu layers on the Mo substrate. This peak is a consequence of the Cu/Mo interface. This conclusion is drawn from the difference in behaviour of the defects in the relaxation phase in the 20 Å Cu/Mo film and those in the ideal Cu crystal. Dislocations leading to the surface are found in the simulated Cu/Mo films starting from a Cu layer thickness of about 20 Å to 25 Å. This is a possible explanation of the decrease of the total trapped fraction in the 75 eV spectrum from about a thickness of 30 Å of the deposited Cu layer. The fact that desorption as in the experiments by heating is not yet feasible in the simulations, introduces a large gap between the outcomes of the simulations and the experimental spectra of the experiments; in the heating the desorption mechanisms and their rates can be quite complex.

Conclusions of a more technical nature can be drawn from the enlargement of the system for the 1000 eV He bombardment. The enhancement of the system in lateral directions does not fully prevent the crossing of the periodic boundaries by the He atoms. The increase of the thickness of the Mo substrate was more successful; the transmission is considerably reduced. For future research in which even thinner Cu layers than the 10 Å Cu + 14 Å Mo film will be bombarded by 75 eV He atoms, it is recommended that the number of planes of the Mo substrate is increased because in the 10 Å run one He atom passes through the thin film.

6.2 Recommendations

In this section follow recommendations for further simulations and TDS experiments organized in subjects.

Subthreshold defect creation

- Ab initio calculations of the He-Cu interaction potential in order to check the present He-Cu interaction.
- TDS experiments with an ideal Cu crystal, employing He fluence variation and subthreshold energy variation, and overlayer experiments to determine the nature of the first peak in the 75 eV spectrum.
- A closer look at stress at interstitially and substitutionally situated He atoms in the simulations with more configurations per period (in this research this has been one configuration in 0.7 ps).

Desorption mechanisms and origin of the peaks

- Experiments to investigate the influence of the temperature ramp to compare the experiments more accurately with the simulations.
- Combination of heating ramp to lower temperatures than 2000 K (for example 800 K in 20 Å Cu/Mo film) and subsequently deposition of overlayers to explore the desorption mechanism of for instance the peak in the 75 eV that is attributed to the interface by the simulations.

- Further analysis of the motion of He atoms, desorption via dislocations and behaviour of the He atoms near the dislocations in the relaxation run of the 20 Å Cu/Mo film after bombardment at 300 K.
- Simulations to gain information on the desorption stage by use of Hyper MD [26], by use of energy minimization as performed by Adams and Wolfer [27] at He atoms in nickel, and by use of Monte Carlo simulations.
- Simulation of 1000 eV He bombardment at 300 K and relaxation at 1200 K with the larger Cu/Mo films (see Sec. 3.1), for this is more realistic than the method used in this work. Such a run can give interesting information about the 1000 eV experiments, though completing the run is necessary (complete fluence). Increasing the number of Cu planes (relatively to the number of Mo planes) and the number of Mo planes will, respectively, add to information gained about the Cu layer and decrease the transmission.
- More general studies of both potential energy and stress in the simulations can give more information about the yet unexplained (by simulations) second peak in 75 eV spectrum and first peak in 1000 eV spectrum.

General recommendations

- As the complexity of the structure of the examined thin films increases, the need to develop an objective instrument by which the local space and thus point defects and other defects in a lattice can be determined will grow. In this research it has been often difficult to determine the volume and size of the defects especially at high temperatures.
- Finally, variation of other parameters in TDS spectra and spectra of ion assisted deposition are of course interesting. Also more simulations of the decoration of the IBAD layers are needed.

References

1) C.-K. Hu, J.M.E. Harper, Materials Chemistry and Physics **52** (1998), pp. 5-16.

2) S.-Q. Wang, MRS Bulletin (Aug 1994), pp. 30-40.

3) C. Ryu, H. Lee et al, Solid State Technology (Apr 1999), pp. 53-56.

4) F.A. Smidt, Int. Mater. Rev. **35** (1990), pp. 61-128.

5) P. Jung and K. Schroeder, J. Nuc. Mat. **155-157** (1988), pp. 1137-1141.

6) R. Smith, *Atomic and Ion Collisions in Solids and at Surfaces*, 1st ed. (Cambridge University Press, Cambridge, 1997), p. 39, 237.

7) P. Klaver, *A Molecular Dynamics Study of Ion Beam Assisted Deposition of Thin Molybdenum Films and Analysis by Thermal Desorption Spectrometry*, (Masters Thesis, Delft University of Technology, 1998).

8) S.M. Foiles, MRS Bulletin **21** (Feb 1996), pp. 24-28.

9) D.J. Oh and R.A. Johnson, in *Proc. of Int. Symp. on Atomistic Simulation in Materials: Beyond Pair Potentials*, edited by V. Vitec and D.J. Srolovitz (1989), pp. 233-238.

10) D.J. Oh and R.A. Johnson, J. Mater. Res. **3** (3) (May/Jun 1988), pp. 471-478.

11) W. Eckstein, *Computer Simulation of Ion-Solid Interactions* (Springer-Verlag, Berlin Heidelberg, 1991), p. 40, 75.

12) G.J. Ackland, G. Tichy et al, Phil. Mag. A **56** (6) (1987), pp. 735-756.

13) R.A. Johnson and D.J. Oh, J. Mater. Res. **4** (5) (Sep/Oct 1989), pp. 1195-1201.

14) Z. Wang, Y. Li and J.B. Adams, Surface Science **450** (2000), pp. 51-63.

15) J.B. Adams, Z. Wang and Y. Li, Thin Solid Films **365** (2000), pp. 201-210.

16) B.S. Bunnik, C. de Hoog, E.F.C. Haddeman and B.J. Thijsse, submitted for publication in Nucl. Instr. and Meth. B (2000).

17) M.I. Baskes, Phys. Rev. B **46** (1992), pp. 2727-2742.

18) M. Paunov and E. Bauer, Appl. Phys. A **44** (1987), pp. 201-208.

19) J. van der Kuur, *Defects in Thin Films deposited with and without Ion Assistance*, (PhD Thesis, Delft University of Technology, 1998).

20) W.Th.M. Buters, *Helium Trapping in Cold Worked Single Crystalline Molybdenum observed with Thermal Desorption Spectrometry*, (PhD Thesis, Delft University of Technology, 1987).

21) E.F.C. Haddeman, B.S. Bunnik and B.J. Thijsse, accepted for publication in Mat. Res. Soc. Proc. (Fall meeting 1999).

22) L.D. van Ee, *The Diffusion Mechanism in Amorphous $Ni_{18}B_{19}$ studied by Molecular Dynamics Simulations*, (PhD Thesis, Delft University of Technology, 1998).

23) T.J. Colla et al., Nuc. Inst. and Meth. in Phys. Res. B **153** (1999), pp. 361-368.

24) A. van Veen, in *Fundamental Aspects of Inert Gases In Solids*, edited by S.E. Donnelly and J.H. Evans (Plenum Press, New York, 1991), pp. 41-57.

25) D.P. van der Werf, *Helium in tungsten, a calculational approach*, (PhD Thesis, Rijksuniversiteit Groningen, 1994).

26) A.F. Voter, Phys. Rev. Let. **78** (20) (19 May 1997), pp. 3908-3911.

27) J.B. Adams and W.G. Wolfer, Journal of Nuclear Materials **158** (1988), pp. 25-19.

Acknowledgements

For this research a number of people have been important, not only in scientific respect: dr. Barend Thijsse, who keeps the fire of the research in the group warm and glowing; Bouke Bunnik who has always time to help someone; ir. Edwin Haddeman who has not been really challenged by the computer problems I encountered and Gerard Bekking, who taught me to rely more on my instincts in physics. Prof. Klapwijk I would like to thank for the advice about the aim of a thesis.
And last, my big friend Patrick to who I am hopelessly in debt in amounts of groceries.

Appendix

The main goal of this appendix is to access all data of the simulation runs for the members of our group. The first table gives an overview of the most used simulations with helium bombardment. The deposition parameters of the configurations at the starting point of the runs are given in Sec. 3.1. The main results are given for a quick overview. Four runs with He bombardment have not been inserted in this table: two tests and bombardment at 1300 K of the 20 Å EVAP and IBAD Cu/Mo film. Run 3503 and 3505 are test runs for respectively 1000 eV and 75 eV helium bombardment. In Sec. 3.3.2 run 3503 is treated. In run 3507 and 3508 20 Å, EVAP and IBAD Cu/Mo films are bombarded by 75 eV He bombardment at 1300 K. Both films randomize during the bombardment and stay randomized after the completion of the bombardment. The results of these runs have been scarcely used in this thesis.
In Table 2 the runs without He bombardment are given. The purpose of these runs was to explore the behaviour of Cu atoms of several films at a certain temperature for example whether surface melting is present. In Sec. 3.3.1 the mean square drift is given for a number of these runs.
Origin of the configurations/data shown in the figures is given in Table 3. The evolution of the research in time can be obtained from the sequence of the run numbers.

Table 1. Overview of the most used simulations with He bombardment.

Implantation phase							
Temperature	300 K			1200 K			
Cu thickness	***Ideal film***	***10 Å***	***20 Å***	***10 Å***	***20 Å***	***20 Å IBAD***	***40 Å***
# Cu	6600	1997	3328	1997	3328	3131	47970
# Mo	0	2160	2160	2160	2160	2154	60480
He energy	75 eV						1000 eV
Run number	3532	3527	3529	3522	3514	3515	3524
# He in	100	100	100	100	100	100	21- until now
Total time (ps)	284	284	284	284	284	284	119
%He Backscattered	78	76	78	84	90	83	43
%He Transmitted	0	1	0	0	0	0	29
%He Left behind in film	22	23	22	16	10	17	29
Cu sputtering yield	0.21	0.23	0.17	0.15	0.21	0.21	0.24
Total Cu Mean Square Drift ($Å^2$)				230.96 (2-284 ps)	213.74 (2-284 ps)		5.25 (4-125 ps)
Defects created	3 V 14 HeV 3 HeV_2 1 He_2V_2 HeV_3 He_2V_3 Rougher surface	9 HeV 3 HeV_2 2 He_2V_2 HeV_3 He_2V_4 2 HeV in Mo 2 He i.s. in Mo	11 HeV 2 HeV_2 2 He_2V_2 He_2V_3 He_3V_4	HeV♦ HeV_2 2 HeV_3 $He_2V_{>5}$ $He_3V_{>9}$ 7 HeV in Mo	4 HeV_2♦ 2 $HeV_{>3}$ $He_4V_{>8}$	6 HeV♦ 3 HeV_2 HeV_3 3 $He_{2/3}V_{>7}$	2 HeV HeV_2 ~10 vac. in Mo♠ 3 He i.s. in Mo

Potential energy (eV)	-3.46 => -3.42	-5.02 => -4.98	-4.65 => -4.62	-4.90 => -4.84	-4.53 =>- 4.46	-4.39 => -4.33	Slight increase, strong oscil- lations ~ -5.15
Comments				Random- ization	Random- ization	Random- ization	
Section	4.3.3	4.3.1	4.2	4.3.1	4.2	4.3.2	4.1
Annealing phase							
Temperature*	1200 K	300 K	1200 K	1200 K			
Run number	3536	3527	3535	3522	3514	3515	3524
Total time (ps)	355	780	355	780	780	780	0
%He Thermal escapes	11	0	14	7	2	5	no info
Total Cu Mean Square Drift ($Å^2$)				222.96 (284- 1064 ps)	104.81 (284- 1064 ps)		no info
Remaining defects	6 HeV 2 HeV_2 $He_3V_{>10}$	No change, see above	4 HeV He_2V_2 $He_2V_{>5}$	$He_2V_{>7}$ 7 HeV in Mo	$He_2V_{>3}$ $He_6V_{>10}$	2 HeV HeV_3 He_2V_6 He_3V_6 $He_4V_{>9}$	no info
Potential energy (eV)	-3.42 => -3.28 => -3.30	-4.98	-4.62 => -4.47 => -4.50	-4.84 => -4.88	-4.46 => -4.51	-4.33 => -4.37	no info
Comments				Recrystal- lization	Recrystal- lization	Recrystal- lization	
Section	4.3.3	4.3.1	4.2	4.3.1	4.2	4.3.2	4.1

*After the implantation of 100 He atoms at 300 K both the ideal Cu crystal and the 20 Å Cu film have been heated in 7.1 ps to 1200 K. The configuration at 294.2 ps is used. The total time these films have been relaxed is somewhat shorter, 355 ps instead of 780 ps. All films bombarded at 300 K have been relaxed for 780 ps; at this low temperature few processes are activated so that these parts of the runs are not very interesting.

♦Vacancies in which the He atoms are given. The copper layer is randomized for most planes; vacancies are not distinguishable.

♠Size of vacancies in Mo is difficult to determine in non-cooled configurations.

i.s. = at interstitial sites, vac. = vacancies

Table 2. Overview of runs without He bombardment.

Thickness (Å)	Method	Temperature (K)	Run number	Period (ps)
10	EVAP	300	3528	106
20	EVAP	300=>1200*	3537	30=>200*
		800	3512	106
		1050	3513	106
		1100	3511	106
		1200	3510	106
		1265	3525	106
		1282	3526	106
		1300	3509	106

40	EVAP	300	3533	14
		1200	3534	106
47	IBAD	1300	3506	106

*The purpose of this run was amongst others to check the temperature ramp that is also performed in runs with He bombardment. Therefore, the 20 Å Cu/Mo film is held for the first 21 ps at 300 K, then the temperature is heightened in 7 ps to 1200 K and after this the film is held another 142 ps at 1200 K.

Table 3. Origin of the configuration/data shown in the figures of this thesis. An 'a' in the name of a configuration means the configuration is cooled. The sites, velocities, accelerations and potential energy against time of all impacted He atoms are usually kept up in the outfile of a run. *Here often parameters of the program 'cn2cn' are mentioned. **Short program for distillation of data.

Figures		***Origin configuration/data***	***Rest operations****
5	EVAP	cn2611a.50000000	cumo symindex
	IBAD	cn2609a.50000000	cumo symindex
7		Several cnfiles of the runs mentioned in the legenda: the zero in the figure is at 30 t*	mean square drift of Cu atoms
8	800 K	cn3512.1500000 & cn3512.300000	disp cumo
	1200 K	cn3510.1500000 & cn3510.300000	disp cumo
	1282 K	cn3526.1500000 & cn3526.300000	disp cumo
	1300 K	cn3509.1500000 & cn3509.300000	disp cumo
9		See 7, cnfiles of run 3510	see 7
10		Outfile of run 3503	x and y-coordinates of He 12527
11		cn3524.1760000	cumo symindex
12	A	cn3532.4040000 & cn3532.30000	disp cumo
	B	cn3529.4040000 & cn3529.30000	disp cumo
	C	cn3514.200000 & cn3514.30000	disp cumo
	D	cn3524.1760000 & cn3524.60000	disp cumo
13	Before	cn3532.30000	cumo symindex / 5th Cu plane
	After	cn3532.4010000	cumo symindex / 5th Cu plane
14		Outfile of run 3524	z-coordinate against time of all He
15		Outfile of run 3524	x and y-coordinates of He
16		Outfile of run 3524 and 3515	lowest z-coordinate of all He atoms
17		cn3524.480000 & cn3524.560000 outfile of run 3524	disp cumo + sites He that impacts at 48 t* from outfile
18		cn3529.15000000 & cn3514.15000000	b.v. cumo symindex
19		cn3529.280000 & cn3529.240000	disp cumo tiny 4
20	300 K	~100 cnfiles of run 3529	'telsprongperimpact'**
	1200 K	~100 cnfiles of run 3514 minus average of run 3510: 92 atoms	'telsprongperimpact'
21	1200 K	~ 200 cnfiles of run 3514a	'totalsymindexofcooledcn'**
	300 K	~ 200 cnfiles of run 3529	'totalsymindexofcooledcn'**
22		Rtfile of run 3529 (300 K), 3514 (1200 K) and 3507 (1300 K)	mean potential energy against time

23	A B	Rtfile of run 3529 (300 K), 3514 (1200 K) and 3535 (300=>1200 K) See 18 and cn3535.5000000	mean potential energy against time
24	Before After	cn3527.30000 cn3527.4000000	cumo symindex cumo symindex
25		cn3527.15000000 & cn3522.15000000	
26	10 Å 20 Å	~ 200 cnfiles of run 3527 ~ 200 cnfiles of run 3529	'totalsymindexofcooledcn'** 'totalsymindexofcooledcn'**
27		cn3527.30000 & cn3527.4040000 (10 Å) cn3529.30000 & cn3529.4040000 (20 Å) cn3532.30000 & cn3532.4040000 (ideal Cu) cn3534.200000 (40 Å)	cnzpl4c
28		cn3529.30000	cumo symindex / 4th Cu plane
29		2609a.50000000	
30		cn3532.15000000 (300 K) & cn3536.5000000 (300=>1200 K)	